UNIVERSITY OF OKLAHOMA

GRADUATE COLLEGE

A DIAGENETIC AND PALEOMAGNETIC STUDY OF THE WOODFORD SHALE, OKLAHOMA, U.S.A.

A THESIS

SUBMITTED TO THE GRADUATE FACULTY

in partial fulfillment of the requirements for the

Degree of

MASTER OF SCIENCE

By

JENNIFER M. ROBERTS
Norman, Oklahoma
2017

A DIAGENETIC AND PALEOMAGNETIC STUDY OF THE WOODFORD SHALE, OKLAHOMA, U.S.A.

A THESIS APPROVED FOR THE
CONOCOPHILLIPS SCHOOL OF GEOLOGY AND GEOPHYSICS

BY

_____
Dr. R. Douglas Elmore, Chair

_____
Dr. Shannon Dulin

_____
Dr. Kurt Marfurt

Acknowledgements

First and foremost, I would like to express my deepest gratitude for the guidance my advisor, Doug Elmore, has given me over the last four years. I am not sure where I would be without his encouragement and support throughout both my undergraduate and graduate studies. Additionally, I would be remiss if I did not acknowledge the impact that many of the other faculty from the School of Geology and Geophysics have had on shaping who I am as scientific professional. They are the reason I have gained more knowledge in the past five years than I could have imagined, and for that I am eternally grateful.

I would also like to thank my many friends and colleagues, with whom I have engaged in many intellectual, productive discussions and whose friendship has made this journey an even better experience. A number of colleagues have contributed significantly to my research through data acquisition and discussions regarding those results, including Brian Cardott, Dr. Mark Curtis, Dr. Andy Madden, and Gerhard Heij. Their time spent aiding my studies has not gone unnoticed and is greatly appreciated. Additionally, I would like to acknowledge the undergraduate laboratory workers for their time spent acquiring my paleomagnetic data, and Chesapeake Energy and Marathon Oil for providing the cores used in this study.

Last but not least, I would like to thank my family and close friends for their endless support in my scholarly endeavors. They have always been there to encourage me through the challenges I have encountered over the last seven years.

Table of Contents

List of Tables

List of Figures

Chapter 1

Chapter 2

Abstract

Two Woodford Shale cores from the Anadarko Basin (Core A, Core C) and one oriented Woodford Shale core from the Ardmore Basin near the Ouachita thrust zone (Core B) were sampled in order to identify diagenetic events, interpret their origin, and uncover the diagenetic history of the shale. Additionally, Core B was examined to test the hypotheses that the Woodford Shale was altered by external, hydrothermal fluids, and contains a magnetization that can be used to date the altering event(s). The Woodford Shale is one of the key hydrocarbon source rocks and unconventional reservoirs in the mid-continent. Understanding the role that diagenetic processes have is fundamental to optimizing our exploitation of the unit.

Thin sections for all cores were analyzed using a variety of methods, such as scanning electron microscopy (SEM) and x-ray computed tomography (XRCT). The shale is extensively altered, exhibiting a complex paragenesis. Multiple fractures and brecciated intervals are common. Early diagenesis is dominated by events in the matrix and allochems, with later diagenesis dominated by events associated with fracturing and brecciation. Cathodoluminescence within fractures reveals evidence of evolving fluids and multiple fluid-flow events. Multiple hydrothermal minerals are present, including biotite, magnesite, norsethite, witherite, gorceixite, potassium feldspar, sphalerite, chalcopyrite, and saddle dolomite. Other minerals present in fractures are albite, apatite, calcite, dolomite, quartz, pyrite, and barite.

Vitrinite reflectance and bitumen reflectance data converted to a vitrinite reflectance equivalent (VRE) reveal trends between thermal maturity and the level of hydrothermal alteration, with Core A (0.80% VR_o (~125°C)) displaying the lowest

alteration, and Cores C (~1.5% VR_o (~210°C)) and B (~1.82% VRo (~230°C)) displaying the highest alteration. Paleomagnetic analysis of Core B reveals the presence of a characteristic remanent magnetization (ChRM) with south-southeasterly declinations and shallow inclinations that is unblocked by 450°C and is interpreted to reside in magnetite. This ChRM is interpreted to be either a chemical remanent magnetization (CRM) or a thermochemical remanent magnetization (TCRM) acquired during the Late Permian. The presence of specimens with the CRM/TCRM in altered rock and the high thermal maturities suggests that this CRM/TCRM originated from alteration by hydrothermal fluids. These results suggest that the Woodford Shale evolved into an open diagenetic system. In addition to causing heightened thermal maturities, these hydrothermal fluids both increased porosity through dissolution and decreased porosity through precipitation of minerals. The Late Permian timing agrees with the dating of hydrothermal alteration found within the Ouachita and Arbuckle Mountains by other workers. The timing for these events is postcollisional, and the most consistent model for the origin of the hydrothermal minerals is fluid flow as a result of faulting that accessed reservoir(s) of warm fluids and facilitated movement.

Introduction to Research

The objective of this study is to characterize the Woodford Shale through an integrated diagenetic and paleomagnetic study. The diagenetic study involves identifying diagenetic events, interpreting their origin, and investigating whether or not there is evidence that the shale was altered by external, hydrothermal fluids. The paleomagnetic study tests the hypothesis that the Woodford contains a magnetization that can be used to date the altering event(s).

This research is separated here into two chapters. Chapter 1 addresses the diagenesis of two cores from the southeastern Anadarko Basin. Chapter 2 discusses the diagenesis and paleomagnetism of a core from the Ardmore Basin. A summary of these chapters can be found following Chapter 2.

Chapter 1: A Diagenetic Study of the Woodford Shale in the Southeastern Anadarko Basin, Oklahoma, U.S.A.: Evidence for Hydrothermal Alteration in Mineralized Fractures

Abstract

The objective of this study is to test if external fluids (e.g., hydrothermal) altered the Woodford Shale in the southeast Anadarko Basin, and how the diagenesis caused by such fluids, particularly in mineralized fractures, has affected the reservoir quality and mechanical behavior of the Woodford Shale. Two Woodford Shale cores from the Anadarko Basin were sampled in order to identify diagenetic events, interpret their origin, and determine the diagenetic history of the shale. Thin sections for both cores were analyzed using reflected and transmitted light, cathodoluminescence, and scanning electron microscopy in order to identify minerals and cross-cutting and textural relationships. X-ray computed tomography was conducted to further characterize fracture networks seen on the petrographic scale. Early diagenesis is dominated by events in the matrix and allochems, with later diagenesis dominated by events associated within fracturing and brecciation. The mineralized fractures and brecciated intervals contain complex mineralogies. Multiple minerals, interpreted to be hydrothermal in origin, are present, including magnesite, norsethite, witherite, gorceixite, potassium feldspar, sphalerite, chalcopyrite, and saddle dolomite. Cathodoluminescence in minerals within fractures reveals evidence of evolving fluids and multiple fluid-flow events. While porosity is present within pyrite framboids, between clay sheets, and dissolution vugs within fractures and allochems, fracture porosity was destroyed by mineralization which filled fractures and permeated into the matrix. Vitrinite reflectance data from both cores

shows a correlation between thermal maturity and level of hydrothermal alteration, with Core A (0.80% VR_o (~125°C)) displaying a lower amount of alteration and Core C (~1.5% VR_o (~210°C)) displaying a higher amount of alteration. The extensive faulting present in the southeastern Anadarko Basin likely facilitated the movement of the hydrothermal fluids through the unit. The presence of hydrothermal minerals not only has implications for the thermal maturity and reservoir quality of the Woodford Shale, but also contributes to the discussion of whether or not shales behave as open or closed systems.

Introduction

The recent growth of unconventional oil and gas plays has sparked a new focus on research into shale characterization. While much progress has been made towards understanding the complexities of these units, questions remain regarding how diagenesis influences reservoir quality and mechanical behavior. Fundamental issues that need to be addressed include whether or not shales behave as open or closed systems as well as how diagenesis impacts migration pathways, porosity, and brittleness (e.g., Elmore at al., 2016).

The Woodford Shale (Late Devonian - Early Mississippian) in Oklahoma is one of the key unconventional reservoirs and hydrocarbon source rocks in the state (Cardott, 2012). The objective of this study is to test if external fluids (e.g., hydrothermal) altered the Woodford Shale in the southeastern Anadarko Basin, and how the diagenesis caused by such fluids, particularly in mineralized fractures, has affected the reservoir quality of the unit (e.g., Dehandschutter et al., 2005; Gale et al., 2014). This study utilizes samples

taken from two Woodford Shale cores from the Anadarko Basin (Fig. 1-1). Thin section petrography, including reflected (RF) and transmitted light (crossed polars (CPO); plane light (PPO)), cathodoluminescence microscopy (CL), scanning electron microscopy (SEM; BSE – backscattered electron imaging, SE – secondary electron imaging), vitrinite reflectance data, and x-ray computed tomography (XRCT) methods are implemented to determine the diagenetic features present, their origin, and their paragenetic sequence with a particular focus on the phases that fill fractures.

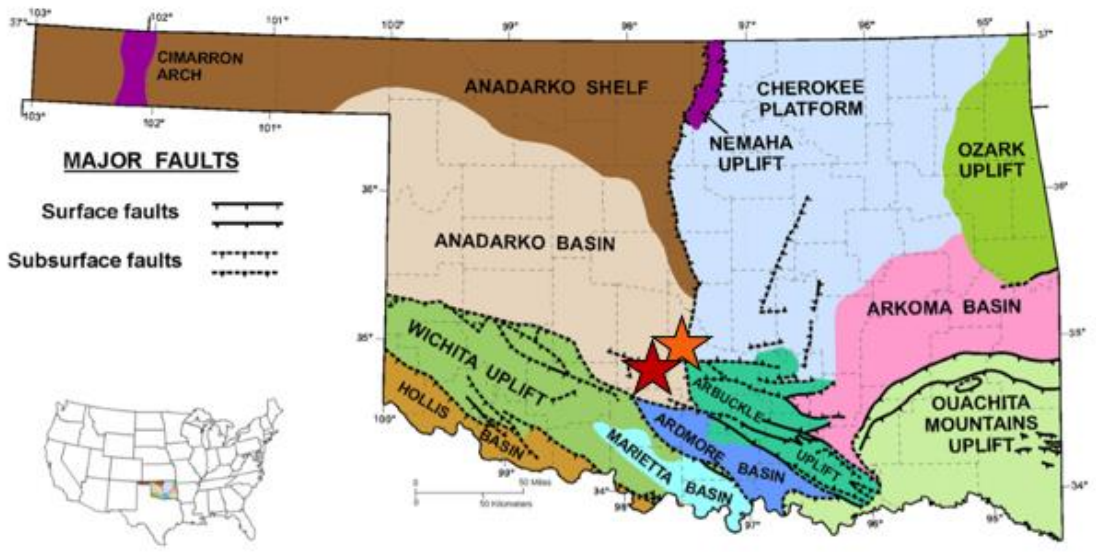

Figure 1-1. Structural provinces of Oklahoma. Normal faults are indicated by the hachures on the downthrown block; thrust faults are indicated by the solid barbs on the hanging wall block. The orange star represents the location of Core A; the red star represents the location of Core C. Modified from Northcutt and Campbell (1998).

Geologic Setting

The Woodford Shale was deposited in the Oklahoma Basin during the Late Devonian-Early Mississippian. During the Late Precambrian to Cambrian, the opening of the proto-Atlantic ocean occurred, resulting in a failed arm of the triple junction known as the Southern Oklahoma Aulacogen (Coffman et al., 1986). The cooling of the aulacogen resulted in a long period of subsidence including the Wichita-Amarillo block lasting between 200 to 250 Ma, subsequently forming the Oklahoma Basin (Robbins & Keller, 1992). As much as 15,000 ft (3,050 m) of sediment were deposited in the Oklahoma Basin from the Late Cambrian through the Mississippian (Johnson, 1989). These sediments consist of thick carbonate sequences interbedded with thinner shales and sandstones, including the Woodford Shale, which were deposited in a marine environment.

The Ouachita orogeny (Late Mississippian-Early Permian) caused both the Wichita and Amarillo blocks to be uplifted and thrust toward the Oklahoma Basin, creating a frontal fault system in the Wichitas along the southwestern edge of what is known today as the Anadarko Basin (Johnson, 1989). This event affected the region from southeastern Oklahoma to the Texas panhandle (Coffman et al., 1986). During this orogenic episode, the Oklahoma Basin was divided into the Anadarko, Ardmore, and Arkoma basins. The Wichita-Amarillo uplift became part of a major structural feature known as the Muenster arch and the Arbuckle uplift was created in south-central Oklahoma. The Ouachita Mountains in southeastern Oklahoma also formed. The Anadarko Basin continued to subside and accumulate sediment into the Guadalupian. The majority of post-Permian strata have since been eroded away (Johnson, 1989).

In the Anadarko Basin, the Woodford unconformably overlies the Hunton Group carbonates and conformably underlies the Osage Lime (Johnson, 1989). Stratigraphically, the Woodford thins to the northwest in the Anadarko Basin (Burruss & Hatch, 1989). Within the Anadarko Basin, thicknesses greater than 900 ft (300 m) can be found along the Wichita fault zone, and depths range from approximately 26,000 to 10,000 ft (7,900 to 3,050 m) in the south-southeast to less than 10,000 ft (3,050 m) in the north-northwest (Cardott & Lambert, 1985).

The Woodford is largely a siliceous black shale or mudstone interbedded with light-colored shale, siltstone, sandstone, dolostone, and chert (Miceli Romero & Philp, 2012). The shale was deposited in a marine environment under primarily anoxic conditions, which, along with slow sedimentation rates and organic productivity, allowed for the preservation of high amounts of organic matter (Miceli Romero & Philp, 2012; Kirkland et. al, 1992). Early diagenetic pyrite, phosphate nodules, and calcite concretions are common, along with scattered siliceous spheres (Miceli Romero & Philp, 2012). The Woodford is quartz-rich making it brittle and highly susceptible to hydraulic fracturing (Cardott, 2012), a characteristic favorable for commercial hydrocarbon exploration. The unconformity present below the Woodford was the result of uplift and erosion of underlying units, creating incised valleys, karst, and subterranean collapse features (Infante-Paez et al., 2017). These topographic irregularities exerted a control on the depositional environments, organic richness, and the occurrence, thickness, and composition of the Woodford.

The southeastern Anadarko Basin, which contains both cores used in this study (Fig. 1-1), directly overlies a portion of what was once the Southern Oklahoma

Aulocogen, whose rifting activity resulted in normal faulting in the area during the Late Precambrian into the Cambrian. Subsidence of the aulacogen made this portion of what is now the southeastern Anadarko Basin part of the primary depocenter for the sediments of the Oklahoma Basin. The Ouachita orogeny resulted in faulting beginning in the Late Mississippian-Early Pennsylvanian and extending into the Early Permian that cross-cut the rocks in this depocenter, including the Woodford Shale. The Wichita frontal fault system bounds the southern edge of the Anadarko Basin. In the southeast, the faulting is dominated by steep, southwest-dipping listric thrust faults which flatten to the southwest. The Arbuckle Mountains also formed at this time, which bounds the southeastern Anadarko Basin to the east. It consists of thrust and strike-slip faulting, the latter of which occurring after the major compressional event and the formation of the Anadarko Basin (Perry, 1989).

Laughrey and Purrazzella (2016) studied the Woodford Shale in the Anadarko Basin, suggesting that diagenesis is an important factor in controlling the reservoir quality. Several other studies have provided information on the diagenesis of the Woodford Shale in the Anadarko Basin (e.g., Chalmers et al., 2012; Cardott, 2013). Berryman (2013) report that the Woodford Shale in the Arkoma Basin contains fractures, commonly filled with calcite. Petrographic, fluid-inclusion, and carbon and oxygen stable-isotopic analyses indicate that multiple fluids were involved in the precipitation of the fracture filling calcite (Berryman, 2013). Other previous studies of mineralized fracture fills in shales and other lithologies include Dehandschutter et al. (2005), Elmore et al. (2015), Elmore et al. (2016), Gale et al. (2014), Heij et al. (2016), and Wu and Olson

(2014). Other studies provide evidence that hydrothermal fluids have altered rocks and can create porosity in carbonates in the southern Midcontinent (Goldstein & King, 2014).

Methodology

Two unoriented vertical cores, Core A and Core C, taken from the southeastern edge of the Anadarko Basin (McClain and Grady counties, respectively) were utilized in this study (Fig. 1-1). Core A contains a Woodford Shale depth range of 9,861-10,051 ft (3,006-3,064 m), and Core C ranges from 13,817-14,030 ft (4,211-4,276 m). While Core A was described in full prior to sampling, Core C samples were taken from 9 sections of core approximately 6 inches long, thus the description is incomplete and the sampling was sparse. Facies descriptions for Core C come from a study conducted by Mann (2014).

Petrographic analysis was conducted on 22 polished thin sections, 12 from Core A and 10 from Core C. Thin sections were chosen based on the representative facies and features such as mineralized fractures. A Zeiss AxioImager.Z1m petrographic microscope accompanied by AxioVision software was utilized for reflected and transmitted light microscopy up to 100x (magnification). An FEI Quantam 250 Scanning Electron Microscope (SEM; BSE – backscattered electron imaging, SE – secondary electron imaging) with a Bruker Electron Dispersive Spectrometer (EDS) was utilized to image and quantify micron scale diagenetic minerals and features. Cathodoluminescence microscopy (CL) was conducted using a Cambridge Image Technology LTD CLmk4 to aid in mineral identification and fracture fill cement paragenesis. Timing of diagenetic events was relative and based on cross cutting and textural relationships as observed in thin sections and on the SEM. X-ray computed tomography scans (XRCT) were

conducted on one inch plugs from each core to further characterize fracture networks and upscale features seen on the petrographic scale. XRCT data for Core A was obtained from the Nano Lab in the Mewbourne School of Petroleum and Geological Engineering. XRCT data from Core C was obtained from the University of Minnesota using a X5000 high resolution microCT system with a twin head 225 kV FeinFocus FXE-225.99 X-ray tube and Dexela 2923 area detector. A Vickers M17 Research Microscope system adapted for reflected white light on slides immersed in oil at a magnification of 500x was used to obtain vitrinite and bitumen reflectance data following the American Society for Testing and Materials guidelines (ASTM, 2014). The bitumen reflectance data was used to calculate vitrinite reflectance equivalent (VRE) values for thermal maturity (Schoenherr et al., 2007; Landis & Castaño, 1994; Barker & Pawlewicz, 1986).

Results and Interpretations

Core A Diagenesis

The stratigraphy of Core A is dominated by siliceous and cherty facies with the next most prominent facies being argillaceous, and the least prevalent being dolomitic and calcareous facies. The lower portion of the core contains largely argillaceous and siliceous lithologies with grey laminae, the middle is dominated by siliceous and cherty lithologies with silty faint laminae, and the upper portion is mostly siliceous with an increased amount of chert that is massive or faintly laminated. Pre-compactional veining is abundant throughout the core. Fracturing is largely sub-vertical in nature and occurs primarily in siliceous and cherty facies.

In Core A, early diagenesis is dominated by events within the matrix and allochems, followed by fracturing and brecciation (Fig. 1-2). The exception to this trend is the abundant pre-compactional veins, which are filled with ferroan dolomite that has been subsequently replaced in some veins by pyrite and fractured during compaction (Fig. 1-3a). Detrital silt-sized quartz is also common throughout the matrix. These grains are sub-angular to sub-round in nature, have a low sphericity, and often display overgrowths. Some detrital quartz grains are replaced by dolomite. The quartz overgrowths are interpreted as early diagenetic in origin (Fig. 1-3b).

Pyrite is abundant and can be found in multiple forms. The majority is interpreted as having formed during early diagenesis. Framboidal pyrite as large as 250 μm (Fig. 1-3c) are present. Both subhedral and euhedral disseminated pyrite is abundant as well and is occasionally concentrated as laminae. Pyrite is also found replacing burrows. Porosity is found in pyrite framboids (Fig.1- 3c) and between clay sheets (Fig. 1-3d).

Radiolaria and Tasmanite cysts are common throughout the shale. The silicification of these allochems by chalcedony, chert, and quartz is common (Fig. 1-3e, f). Some of these allochems are replaced by calcite, dolomite, and pyrite (Fig. 1-3f). Apatite also replaces Tasmanites. Mollusks that have undergone inversion to from aragonite to calcite, and subsequently altered to dolomite, are also present (Fig 1-4a). With the exception of apatite and magnesite, the occurrences of diagenetic events within allochems are interpreted as early. Dissolution vugs are also found within allochems (Fig. 1-3f).

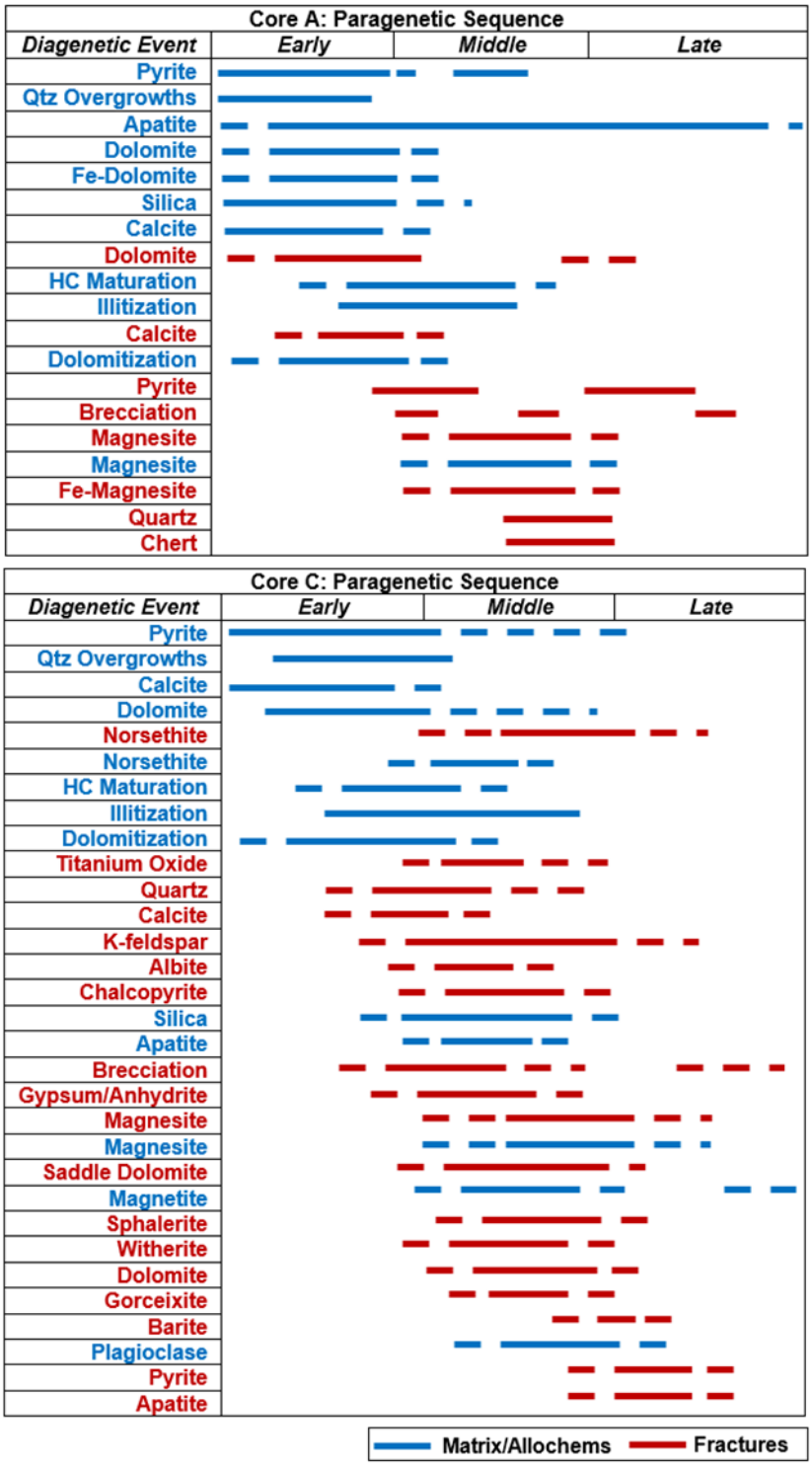

Figure 1-2. Paragenetic sequences for Core A and Core C. Events are listed from early to late. Timing is based on cross-cutting and textural relationships. Events in blue occur within the matrix and allochems, while events in red occur in the fracture fills. Dashed line refers to uncertainty in timing.

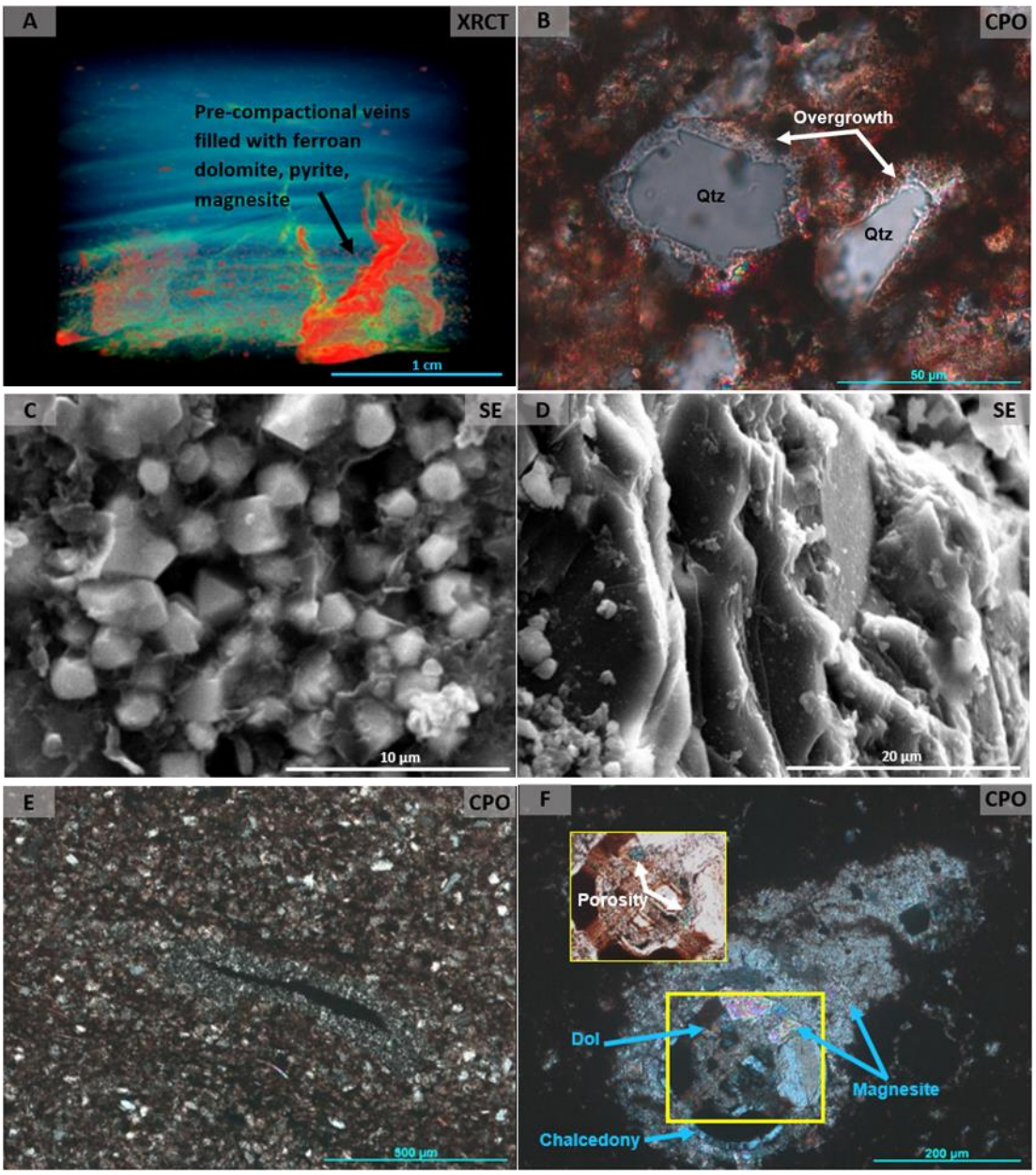

Figure 1-3. Various early diagenetic features within Core A. A) XRCT scan displaying pre-compactional veining of ferroan dolomite, magnesite (middle to late), and pyrite. Also note microfractures which are not obvious in core descriptions. Cool colors (green, blue) represent low densities; warm colors (yellow, red) represent high densities. B) Detrital quartz (Qtz) grains with overgrowths. C) SEM (SE) image of a pyrite framboid in the matrix containing porosity. D) SEM (SE) image of porosity found between clay sheets. E) Chert-replaced Tasmanite in a dolomitic mudstone facies oriented along burrowing present at ~45° angle. F) Radiolarian partially replaced by chalcedony, dolomite, and magnesite. The inlaid image indicated by the yellow box taken under plane polarized light highlights the dissolution porosity found within the allochem, seen as blue epoxy. (*XRCT = x-ray computed tomography; CPO = crossed polarized light; SE = secondary electron image)*

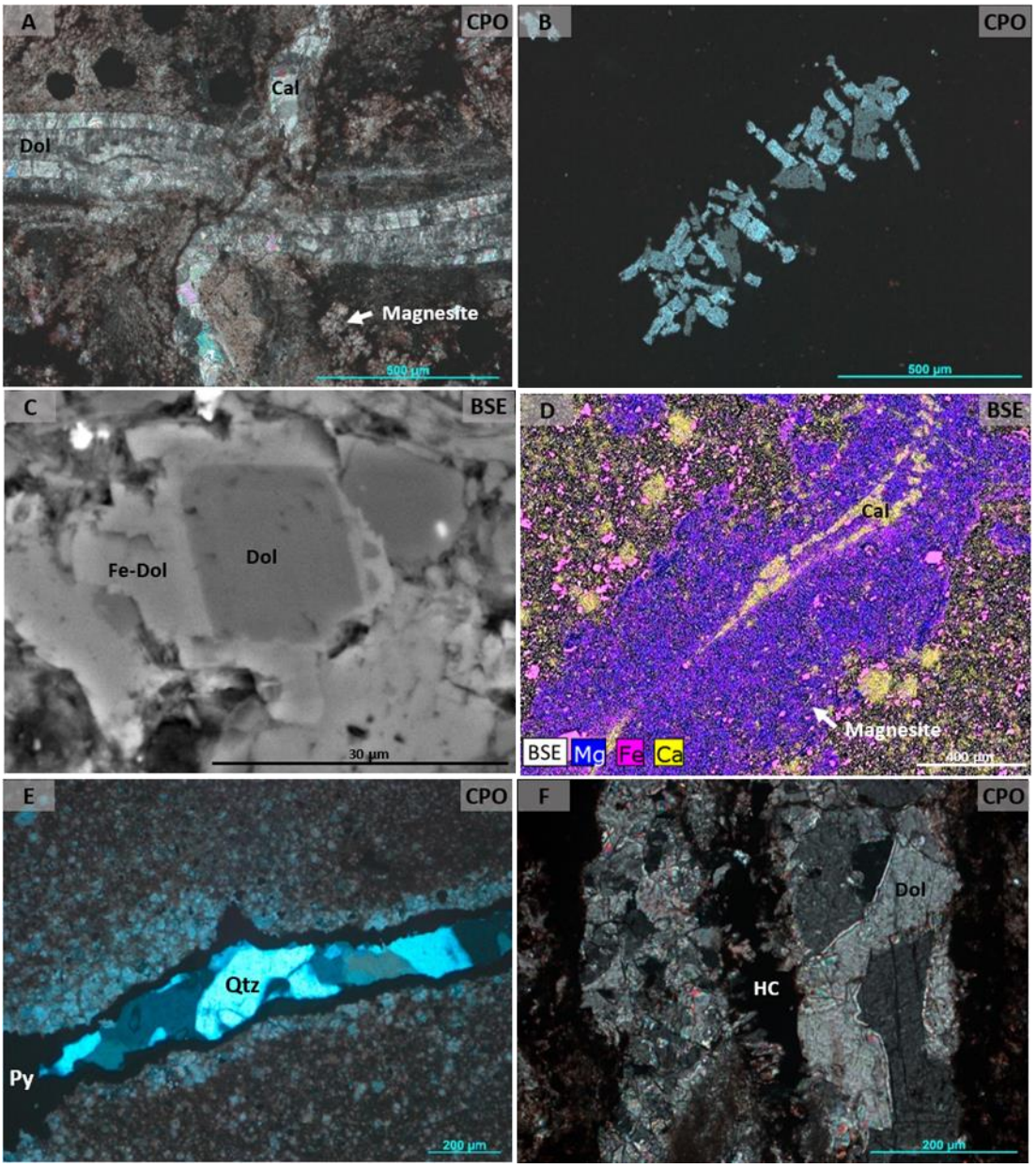

Figure 1-4. Diagenetic features within Core A. A) Mollusk that inverted from aragonite to calcite, then altered to dolomite with magnesite permeating the surrounding matrix being cross-cut by a calcite fracture. B) Aggregate of tabular apatite crystals in the matrix. C) Detrital dolomite grain with an authigenic ferroan dolomite rim growing into the surrounding porosity. D) SEM (BSE) image with an EDS overlay indicating mineral composition. A calcite fracture is in yellow with ferroan magnesite in blue found within the fracture and the surrounding matrix. E) Fracture filled with pyrite (Py) and megaquartz (Qtz). F) Dolomite (Dol) filled fracture with bitumen or hydrocarbons (HC) in the center. (*SEM = scanning electron microcopy; EDS = elemental dispersive analysis; BSE = backscatter electron image; CPO = crossed polarized light)*

Apatite is also present in the matrix as aggregates of tabular crystals (Fig. 1-4b), likely due to the dissolution and reprecipitation of phosphatic material. Overgrowths containing ferroan dolomite on rounded non-ferroan dolomite grains interpreted to be detrital, are present (Fig. 1-4c).

Authigenic clay, interpreted as illite based on energy dispersive analysis, is present in the matrix. The illite is interpreted to have formed from smectite during late early to middle diagenesis. Maturation of hydrocarbons probably occurred at approximately this time as well (Pevear, 1999).

Fractures observed in the core are dominantly vertical to sub-vertical in nature, and there is evidence of fracture related brecciation events (Fig.1- 4a, d-f). The XRCT scans indicate the presence of microfractures which are not obvious from core descriptions (Fig. 1-3a). Porosity occurs as dissolution vugs in fractures and within brecciated intervals. The dominant minerals in the fractures are dolomite and calcite based on thin section and SEM observations. Less commonly, fractures are filled with euhedral pyrite, megaquartz, chert, and bitumen (Fig, 1-4e, f). Magnesite ($MgCO_3$), was interpreted to be present based on energy dispersive analysis. It is found throughout the core in fractures, permeating into the matrix surrounding fractures and veins, and in allochems (Fig.1-3a, f; Fig.1- 4a, d).

A total of 23 vitrinite reflectance measurements yield an average value of 0.80% VR_o for Core A. Additionally, four bitumen reflectance values yield average vitrinite reflectance equivalent (VRE) values of 0.88% and 0.76%, utilizing conversion equations from Landis and Castaño (1994) and Schoenherr and others (2007), respectively. These

data equate to a maximum heating temperature of approximately 125°C (Barker & Pawlewicz, 1986).

Core C Diagenesis

The stratigraphy of Core C is dominated by mudstone, siliceous mudstone, and bioclastic mudstone facies with a moderate amount of chert beds and lesser amounts of silty mudstone. The lower portion of the core is characterized by siliceous and organic-rich mudstone facies with interbedded silty mudstone. The middle section is dominated by mudstones, siliceous mudstones, and increasing bioclastic mudstones up section. The upper portion is characterized by bioclastic mudstone facies with abundant barite-rich laminae and less frequent mudstone and siliceous mudstone facies. Chert beds are most dominant in the lower and middle portions of the core. While unconfined fracture networks do exist, fractures are most often confined to siliceous and cherty facies (Mann, 2014).

Although the paragenesis of Core C is more complex than that of Core A (Fig. 1-2), the trend of matrix and allochem events dominating early diagenesis and fracturing events dominating later diagenesis are the same in both cores. An exception is the pre-compactional veins filled with norsethite ($BaMg[CO_3]_2$); interpreted as replacement after calcite or dolomite during middle diagenesis in Core C (Fig. 1-5a).

Pyrite is present in various forms, including framboids and disseminated crystals in the matrix as well as euhedral crystals that have replaced allochems such as radiolaria and Tasmanites. Prior to the pyritization of these allochems they are typically replaced partially or entirely by calcite, dolomite, or a form of silica (Fig. 1-5b). At approximately

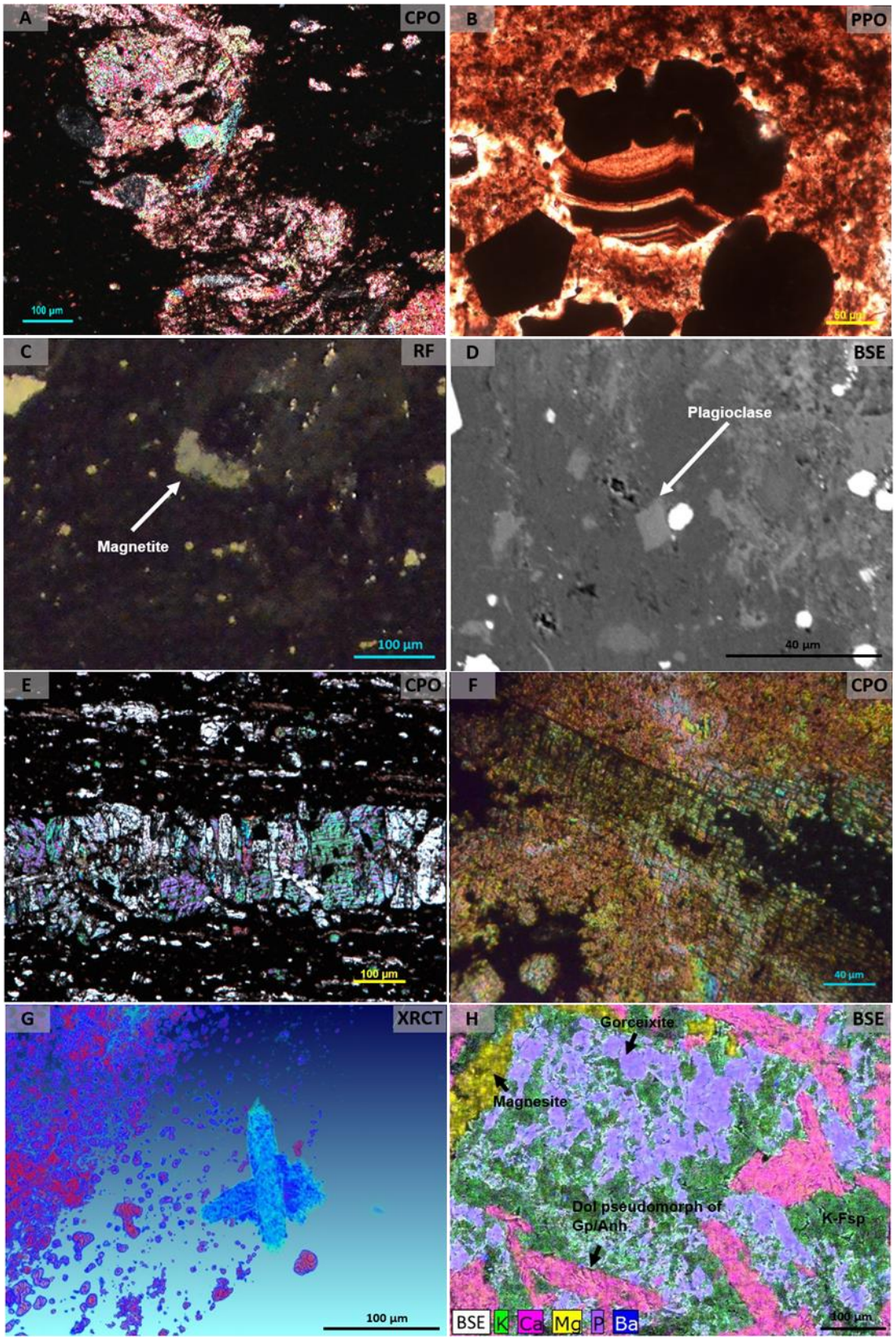
A
CPO
100 µm
B
PPO
C
RF
Magnetite
100 µm
D
BSE
Plagioclase
40 µm
E
CPO
100 µm
F
CPO
40 µm
G
XRCT
100 µm
H
BSE
Gorceixite
Magnesite
Dol pseudomorph of Gp/Anh
K-Fsp
BSE K Ca Mg P Ba
100 µm

Figure 1-5. Diagenetic features within Core C. A) Pre-compactional vein filled by norsethite, interpreted as a replacement of calcite or dolomite. B) Chalcedony-filled radiolarian being replaced by euhedral pyrite. C) Authigenic magnetite crystal in the matrix. D) SEM (BSE) image of an authigenic plagioclase crystal in the matrix. E) Horizontal calcite fracture displaying a "beef" texture. F) Saddle dolomite in a fracture. G) XRCT image of a dolomite pseudomorph of gypsum displaying a fishtail twin. Cool colors (green, blue) represent low densities; warm colors (yellow, red) represent high densities. H) SEM (BSE) image of fracture fill with an EDS overlay indicating mineral composition. The pink phase is dolomite (Dol) pseudomorphs of gypsum (Gp) or anhydrite (Anh), the blue is gorceixite, the green is potassium feldspar (K-Fsp), some of which containing Ba, and the yellow is magnesite. ***(CPO = crossed polarized light; PPO = plane polarized light; RF = reflected light; SEM = scanning electron microcopy; EDS = elemental dispersive analysis; BSE = backscatter electron image; XRCT = x-ray computed tomography)***

the same time these events occur during early diagenesis, overgrowths on detrital quartz, as in Core A, are interpreted as having formed (e.g., Schieber et al., 2000). Similar to Core A, porosity is found in pyrite framboids and between clay sheets.

Authigenic illite is found in the matrix, and the smectite to illite transformation is interpreted to have occurred during the latter portion of early diagenesis and during middle diagenesis. Other diagenetic events that occurred within the matrix, such as dolomitization and the maturation of hydrocarbons, are interpreted to have occurred during early and middle diagenesis. Authigenic magnetite is also found in the matrix (Fig. 1-5c), along with elongate authigenic apatite crystals as large as 1 mm in length, and euhedral plagioclase crystals (Fig. 1-5d).

Fracturing is dominantly sub-vertical in nature and contains a complex suite of minerals. Dissolution vugs are present within fractures. The sparse horizontal fractures are commonly associated with the brecciation events, and is the only location that cone-

in-cone and beef calcite fracture fills are found (Fig. 1-5e). These beef type fractures are filled with fibrous calcite that is oriented vertically, perpendicular to fracture walls.

Other carbonate minerals commonly found in the shale are dolomite, as well as magnesite, norsethite, and less commonly witherite ($BaCO_3$) that are interpreted to be present based on energy dispersive analysis. Dolomite occurs as fracture filling, including saddle dolomite (Fig. 1-5f), and as pseudomorphs of gypsum or anhydrite within both fractures and the matrix (Fig. 1-5g, h; Fig.1-6a). Dolomite is interpreted as occurring in the matrix and allochems during early to middle diagenesis, and in fractures during middle-late diagenesis. Similarly to Core A, magnesite and norsethite occur as both fracture filling and in the matrix (Fig.1-5a, h; Fig. 1-6a-c). Witherite occurs in euhedral form within fractures (Fig. 1-6d). Magnesite, norsethite, and witherite are interpreted as occurring during middle-late diagenesis.

Fractures also contain other barium-bearing minerals such as barite, gorceixite ($BaAl_3(PO_4)(PO_3OH)(OH)_6$), and barium-potassium feldspar (Fig. 1-5h). Other forms of feldspar, including potassium feldspar without barium (Fig. 1-5h), and albite (Fig. 1-6e) are present. Bitumen is also present filling porosity in fractures (Fig. 1-6e). Quartz in fractures occurs in association with the feldspar, and also as euhedral crystals growing from fracture walls. Later stage fracture fills include pyrite and apatite. While quartz is interpreted as occurring in fractures from early to middle diagenesis, barite, gorceixite, potassium feldspar, albite, pyrite, and apatite are interpreted as occurring during middle-late diagenesis (Fig. 1-5h; Fig. 1-6a, e).

Ore minerals such as sphalerite, chalcopyrite, and titanium oxides are found around fractures (Fig. 1-6f). Chalcopyrite occurs as a core within a sphalerite mass.

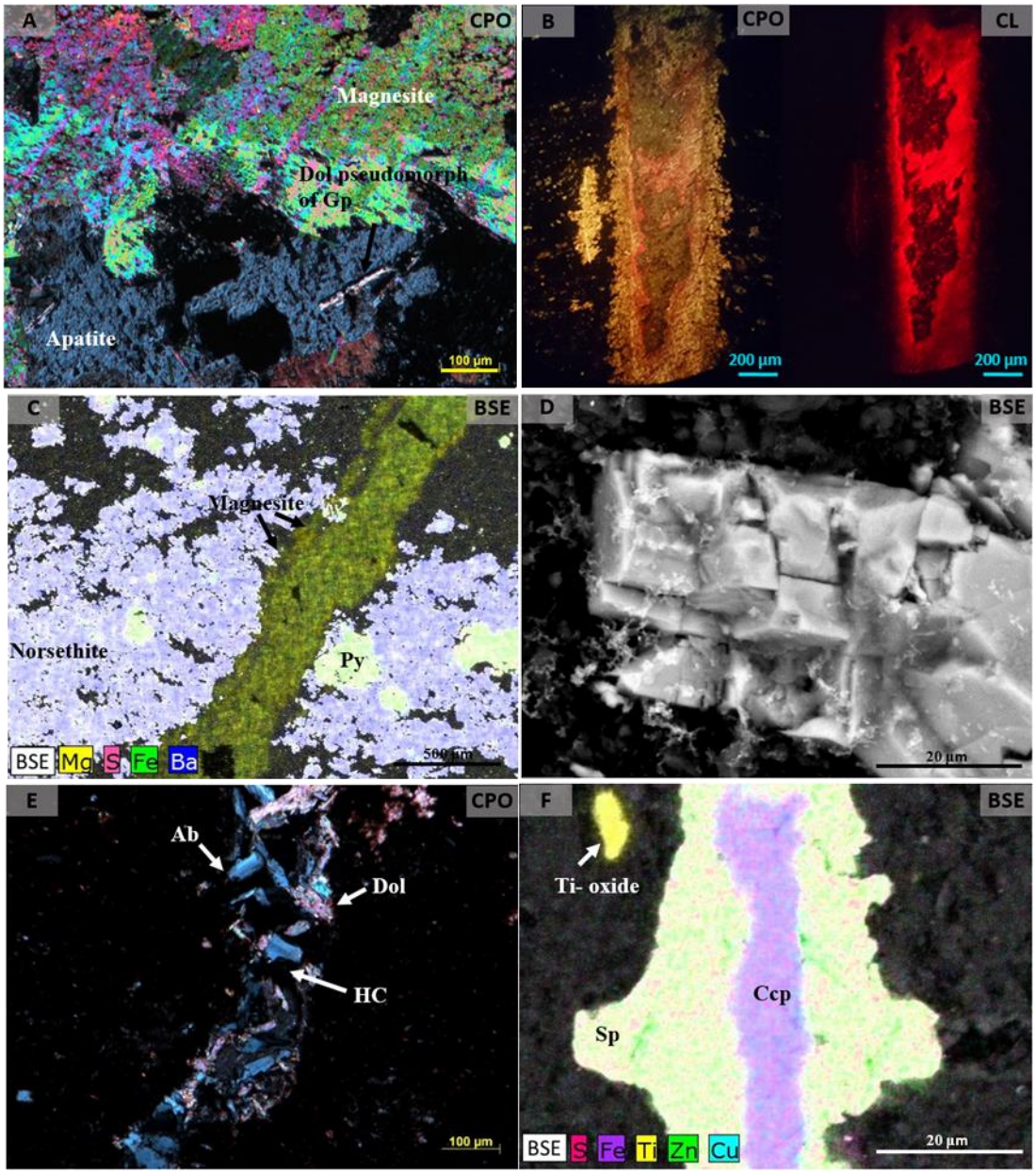

Figure 1-6. Diagenetic features within Core C. A) Magnesite being replaced by apatite, which is subsequently being replaced by bladed dolomite pseudomorphs of gypsum. B) Twin CPO and CL images of a dolomite fracture with ferroan magnesite permeating the matrix and dissolution in the center. Note that the dolomite luminesces and the ferroan magnesite does not. C) SEM (BSE) image with EDS overlay indicating mineral composition. Norsethite in the matrix is in blue, pyrite is in green, and the fracture cutting through this feature is magnesite in yellow. D) SEM (BSE) image of witherite in a fracture. E) Fracture with albite (Ab) and dolomite (Dol) with bitumen or hydrocarbons (HC) in the pore space. F) SEM (BSE) image with an EDS overlay indicating mineral composition. The purple is chalcopyrite (Ccp), the green is sphalerite (Sp), and the yellow is a titanium oxide.

(CPO = crossed polarized light; CL = cathodoluminescence; SEM = scanning electron microcopy; EDS = elemental dispersive analysis; BSE = backscatter electron image).

Titanium oxides are found within and on the edges of fractures. Sphalerite, chalcopyrite, and the titanium oxides are interpreted as occurring during middle diagenesis.

Vitrinite reflectance data yields an approximate value of 1.5% VR_o for Core C. This equates to a maximum heating temperature of approximately 210°C (Barker & Pawlewicz, 1986).

Discussion

Both cores display extensive alteration based on the presence of abundant fracturing, brecciation, and veining (e.g., Fig. 1-4a, f). The recognition of wide variety of fracture mineralogies paired with cathodoluminescence suggests this rock encountered multiple fluid-flow events with different fluid chemistry (Fig. 1-6b).

Silica replacement of microfossils is interpreted to be early based on textural relationships (Schieber et al., 2000). Most of the pyrite is interpreted to be early diagenetic in origin and probably formed as a result of the sulfate reduction process (Schieber, 2011). Horizontal pyrite laminae probably represent either areas of enriched organic matter or a flux of detrital iron deposition (Berner et al., 1985). The authigenic magnetite found in the matrix probably formed from altering fluids, clay diagenesis, or the maturation of organic matter (e.g., Katz et al., 2000; Blumstein et al., 2004; Elmore et al., 2012), and is interpreted as occurring during middle and late diagenesis. The fractures filled with cone-

in-cone and “beef” calcite (Fig. 1-5e) are interpreted to have formed relatively early, and may have precipitated as a result of tensile, bedding-parallel fracturing during compaction and dewatering (Maher et al., 2017) or as a result of overpressuring (e.g., Cobbold et al., 2013).

There are multiple minerals present that indicate the Woodford has been altered by hydrothermal fluids during middle-late diagenesis. Saddle dolomite (e.g., Williams, 2015), magnesite, norsethite, witherite, gorceixite, potassium feldspar, sphalerite, chalcopyrite, apatite, and albite have been tied to hydrothermal activity. While magnesite can form in a variety of ways, the mostly likely origin of crystalline magnesite in the Woodford is through an influx of hydrothermal magnesium-rich fluids having derived its magnesium from underlying dolomites (Shand, 2006). Norsethite is known to form in hydrothermal environments (e.g., Bötcher, 2000; Steyn & Watson, 1967). Witherite is believed to form as a result of hydrothermal alteration associated with barite (e.g., Chamberlain et al., 1986). Gorceixite has been linked to hydrothermal and volcanic activity, notably in carbonaceous argillic shales (e.g., Migaszewski et al., 2007). Shelton and others (1986) reported potassium feldspar, specifically barium-rich adularia, within the Womble Shale of the Ouachita Mountains in Arkansas, and related it to postcollisional hydrothermal activity. This is particularly interesting due to the role that the Ouachita orogeny had in forming the Anadarko Basin. The Mississippi Valley-type sphalerite and chalcopyrite deposits can be hydrothermal in origin (e.g., Leach & Rowan, 1986). Additionally, apatite has been tied to hydrothermal alteration (e.g., Bouzari et al., 2016). Kastner (1971) points out that albite can form at low temperatures with an internal source for the ions or an external source such as migrating saline fluids. Albite could have formed

from alkaline fluids that altered illite and quartz, resulting in Al and Si-rich fluids from which albite can precipitate (Poole et al., 2014), or during the illitization of smectite.

Core C contains nearly all of the same diagenetic features as are present in Core A, with the exception of chert in fractures and ferroan dolomite overgrowths on detrital dolomite (Fig. 1-4c). Allochem and matrix diagenesis is almost identical between the two except for the plagioclase, magnetite, and norsethite present in Core C that have not been identified in Core A. Core C, however, has a much more complex fracture paragenesis. The majority of the hydrothermal minerals found in this study reside in Core C, which also has the greater thermal maturity based on the vitrinite reflectance data. When comparing the maximum depths of both cores to a burial versus vitrinite reflectance curve for the Woodford Shale in the Anadarko Basin from Cardott and Lambert (1985), the VR_o value for Core A is consistent with estimated values while the VR_o for Core C is slightly elevated. Here, hydrothermal fluids are defined using the convention proposed by White (1957), as "*aqueous solutions that are warm or hot relative to the surrounding environment*", and temperatures 5-10°C higher than the host rock are considered significant (Machel & Lonnee, 2002; Stearns et al., 1935). This allows the term to be applied to diagenetic systems.

Many of the minerals found in the Woodford have been reported from rocks that have not been affected by hydrothermal fluids. Examples are albite (Kastner, 1971; Poole et al., 2014), norsethite (Mrose et al., 1961), and barite (Selleck, 2014; González-Muñoz et al., 2003). In these cases, the elements in these minerals were interpreted to come from internal sources in the shales. The preponderance of evidence, including the number of

minerals that could be of hydrothermal origin, suggests that Woodford fractures were mineralized by such fluids.

It is also possible that many of the elements found in the hydrothermal minerals in the fractures and surrounding matrix could have been leached from the shale, however, it is unlikely that all of them were. Based on the petrographic and SEM evidence, the hydrothermal fluids only locally altered the shale around the mineralized fractures. Hydrothermal mineralization is mostly focused within the siliceous and cherty facies that are prone to the largest amount of fracturing. This suggests that fractures were the primary migration pathway for the warm fluids.

There is abundant evidence that hydrothermal fluids have altered the Woodford Shale in the cores. Multiple hydrothermal minerals are present in fractures which might suggest one fluid migration event. However, in some cases minerals are found in cross-cutting relationships (Fig. 1-6c) documenting hydrothermal events.

The diagenesis has also exerted an influence on the reservoir quality of the unit. Porosity in the Woodford Shale is observed in pyrite framboids, associated with clays, and within dissolution vugs in fractures and allochems, which may have been caused by the hydrothermal fluids. Most of the fracture porosity was occluded by the precipitation of hydrothermal minerals in and surrounding the fractures. Examples of this are the mineralization of magnesite and norsethite in the matrix surrounding the fractures (Fig. 1-3a, f ; Fig. 1-4a, d; Fig. 1-6a-c), and the growth of minerals in fractures (e.g., dolomite, calcite, quartz, magnesite, and norsethite). The growth of ferroan dolomite into the pore space around detrital dolomite grains also occluded porosity (Fig. 1-4c). Additionally, the migration and deposition of bitumen also occluded pores (e.g., Figs. 1-4f, 1-6e).

As previously stated, the siliceous and cherty facies contain the highest amount of natural fractures. Some of the diagenetic minerals such as quartz, feldspar, dolomite, and calcite can promote additional brittle behavior (Jin et al., 2015). Intervals with numerous fractures where hydrothermal minerals (e.g., magnesite) have permeated into the matrix could influence the geomechanical properties. We acknowledge the geomechanical properties are dependent on more than just mineralogy (e.g., fracture toughness; Jin et al., 2015). The XRCT data allows for the characterization of complex fracture networks which were not observed during thin section and SEM examination, and could relate to brittleness (Jin et al., 2015). These data also reveal information on fracture geometry and mineralogy. Characterizing natural fractures is also important because they may influence hydraulic fracturing (e.g., Olson & Dahi-Taleghani, 2010). Developing a better understanding of these fracture characteristics can yield information that could aid in identifying intervals that may be good targets for hydraulic fracturing or intervals to avoid.

The hydrothermal fluids may also have increased the thermal maturity in the Woodford Shale, at least locally. This may have resulted in cracking of the hydrocarbons and the formation of bitumen which filled pores in the shale. This process, however, could lead to gas formation and may also create porosity in organic matter (e.g., Misch et al., 2016). The fact that hydrothermal fluids altered the Woodford, at least locally, introduces uncertainty in exploration as it pertains to thermal maturity and the destruction of porosity and permeability by mineralization.

The issue of open versus closed remains an important question in shales (e.g., Bjorlykke & Jahren, 2012; Land et al., 1997). The evidence that the cores have undergone

hydrothermal alteration suggests the Woodford Shale evolved into an open system to external fluids during middle to late diagenesis when the minerals in the fractures precipitated. During early diagenesis when silica replaced microfossils and most of the pyrite formed, the Woodford was probably largely closed to external fluids. Faults and most of the mineralized fractures probably formed during the Ouachita orogeny in the Late Paleozoic, which provided the conduits for the external hydrothermal fluids.

The most likely mechanism for this influx of hydrothermal fluids is through fault-related activity. Both cores are located within the southeast portion of the Anadarko Basin, which is where it is deepest and where it is bounded by the Wichita frontal fault system and Arbuckle structural features. The Ouachita orogeny that formed these structures produced faulting within the Woodford formation where these features meet the Anadarko Basin (Perry, 1989), likely providing potential conduits for fluid flow. Sharp (1978) proposed that faults in the Ouachita Basin may have provided conduits for fluids that precipitated MVT mineralization in northern Arkansas and southeastern Missouri. Shelton and others (1986) reported hydrothermal activity in the Womble Shale of the Ouachita Mountains, and suggested that post-folding faulting accessed a reservoir of warm fluids, resulting in their migration through existing fault networks. Additionally, a significant amount of faulting separates Cores A and C from one another (Marsh & Holland, 2016). If a significant amount of these faults are sealing, this could provide an explanation for the differences in amounts of hydrothermal alteration between the cores.

Conclusions

The Woodford Shale in two cores from the southeastern Anadarko Basin has been extensively altered by hydrothermal minerals. Minerals interpreted as hydrothermal in origin include witherite, norsethite, magnesite, saddle dolomite, gorceixite, potassium feldspar, chalcopyrite, sphalerite, and potentially albite and apatite. The most likely mechanism for this hydrothermal activity is faults which are common in the southeastern Anadarko Basin. The diagenesis has influenced reservoir properties such as the creation of porosity through dissolution and the destruction of porosity through the mineralization by permeating fluids. Authigenic minerals might have contributed to the brittleness of the rock, ultimately affecting the efficiency of hydraulic fracturing. The evidence of hydrothermal alteration has important implications in oil and gas exploration and is also important in terms of the whether shales are open or closed. The evidence suggests that the Woodford has been an open system at some time in its diagenetic history.

Chapter 2: Hydrothermal Alteration in the Woodford Shale, Oklahoma, U.S.A.

Abstract

An oriented Woodford Shale core from the Ardmore Basin near the Ouachita thrust zone was obtained in order to test the hypotheses that the Woodford Shale was altered by external, hydrothermal fluids, and contains a magnetization that can be used to date the altering event(s). The shale is extensively altered and contains a complex paragenesis. Multiple fractures, both early and late, as well as brecciated intervals, are common. Fractures and parts of the matrix contain authigenic minerals which are interpreted as originating from hydrothermal alteration, such as biotite, magnesite, norsethite, gorceixite, and potassium feldspar. Additionally, there are numerous quartz-filled fractures associated with altered intervals in the core. Numerous fractures contain pyrobitumen displaying vitrinite reflectance equivalent (VRE) values of up to 1.57%, and sparse vitrinite reflectance data yields a mean of 1.82% VR_o. These values equate to alteration temperatures of approximately 210-230°C. Paleomagnetic analysis reveals the presence of a characteristic remanent magnetization (ChRM) with south-southeasterly declinations and shallow inclinations that is unblocked by 450°C and is interpreted to reside in magnetite. This ChRM is interpreted as a chemical remanent magnetization (CRM) or a thermochemical remanent magnetization (TCRM) acquired during the Late Permian. The presence of specimens with the CRM/TCRM in altered rock and the high thermal maturities suggests that this CRM/TCRM originated from alteration by hydrothermal fluids. These results suggest that the Woodford Shale evolved into an open diagenetic system in its history. In addition to causing heightened thermal maturities,

these hydrothermal fluids both increased porosity through dissolution and decreased porosity through precipitation of minerals. The Late Permian timing agrees with the dating of hydrothermal alteration found within the Ouachita and Arbuckle Mountains by other workers. The timing for these events is postcollisional, and the most consistent model for the origin of the hydrothermal minerals is fluid flow as a result of faulting that accessed reservoir(s) of warm fluids and facilitated movement.

Introduction

The Woodford Shale (Late Devonian-Early Mississippian) has become one of the most important source rocks and unconventional reservoirs in Oklahoma (Cardott, 2012). The proliferation of unconventional reservoirs has led to research indicating shales are much more complex than previously thought. While much progress has been made towards understanding the depositional and stratigraphic complexities (e.g., Turner et al., 2016; Milliken et al., 2012; Schieber et al., 2000; Slatt & Rodriguez, 2012), how diagenesis impacts shales is still not as well understood (e.g., Elmore et al., 2016). One fundamental issue that needs to be addressed is whether shales are open or closed systems (e.g., Bjorlykke & Jahren, 2012; Land et al., 1997).

The purpose of this study is to determine the paragenesis, timing, and origin of diagenetic events in the Woodford Shale. A key objective is to test the hypothesis that the Woodford Shale was altered by external, hydrothermal fluids. A second hypothesis is to test if the shale contains a chemical remanent magnetization (CRM) that can be used to date the altering event(s).

This study utilizes samples taken from an oriented core in the Ardmore Basin (Core B, Fig. 2-1). A diagenetic study was conducted using scanning electron microscopy (SEM), cathodoluminescence microscopy (CL), reflected and transmitted light microscopy, and x-ray computed tomography (XRCT) imaging. Paleomagnetic methods were employed to isolate a remagnetization that could be used to date diagenetic events.

Geologic Setting

The Ardmore, Anadarko, and Arkoma Basins in Oklahoma (Fig. 2-1) were previously a part of the encompassing Oklahoma Basin (Robbins & Keller, 1990). The basin formed as a result of subsidence by the failed arm of a rifting event that occurred during the Late Precambrian-Cambrian called the Southern Oklahoma Aulacogen (Coffman et al., 1986). Between the Late Cambrian and the Mississippian as much as 15,000 ft (3,050 m) of mostly carbonate and shale sequences were deposited in the Oklahoma Basin, including the Woodford Shale (Robbins & Keller, 1990). The basin was divided into sub-basins by the Ouachita orogeny that began in the Late Mississippian-Early Pennsylvanian and extended into the Early Permian (Johnson, 1989), affecting the region from southeastern Oklahoma to the Texas panhandle (Coffman et al., 1986). Structural features dividing these basins include the Wichita-Amarillo uplift in the southwest, the Arbuckle uplift in the south, and the Ouachita Mountains in the southeast (Johnson, 1989).

The Woodford unconformably overlies various formations across Oklahoma, including the Simpson Sandstone (Middle Ordovician), the Viola Limestone (Middle-Late Ordovician), the Sylvan Shale (Late Ordovician), and the Hunton Group carbonates

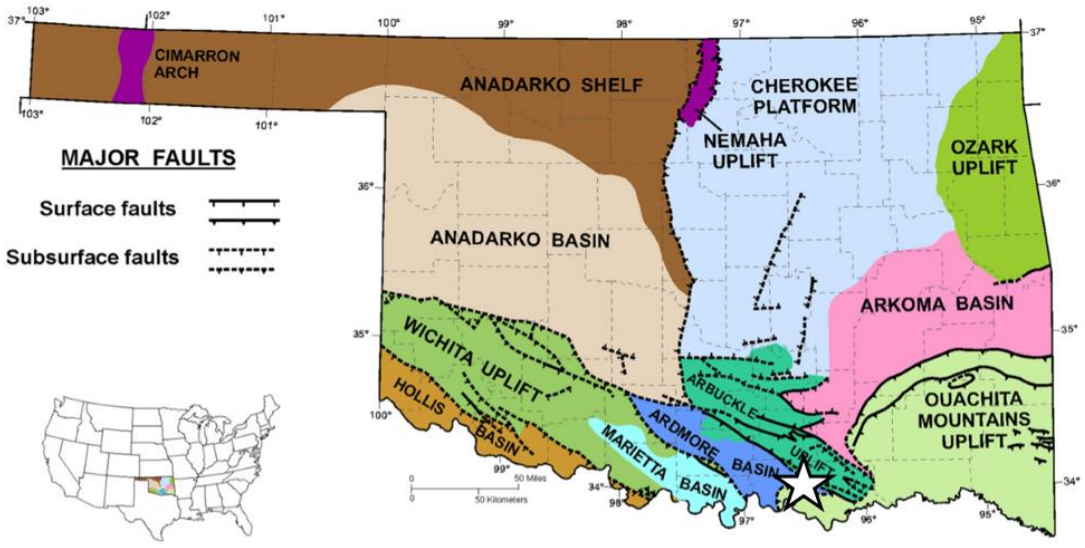

Figure 2-1. Structural provinces of Oklahoma. Normal faults are indicated by the hachures on the downthrown block; thrust faults are indicated by the solid barbs on the hanging wall block. The star indicates the location of Core B. Modified from Northcutt and Campbell (1998).

(Silurian-Devonian), and is conformably overlain by Mississippian limestones and the Caney Shale (Middle Mississippian) (Boyd, 2008; Infante-Paez et al., 2017). Thickness variations of the Woodford can be attributed to the irregular topography caused by subaerial exposure of the underlying rock. Thicknesses tend to be thicker (>100 ft (30 m)) when overlying the less resistant Sylvan and Simpson units, and thinner (<100 ft (30 m)) when overlying the more resistant Hunton Group and Viola units (Infante-Paez et al., 2017).

The Woodford is an organic-rich, siliceous black shale with interbedded light-colored shale, siltstone, dolostone, and chert (Miceli Romero & Philp, 2012) deposited in restricted marine, hypersaline, and potentially lacustrine environments (Infante-Paez et al., 2017). The high organic content present in the Woodford is due to the primarily anoxic conditions it was deposited under and slow sedimentation rates (Kirkland et al., 1992), with its variability caused by sea-level fluctuations and topographic relief influencing ocean circulation and oxygenation during deposition (Infante-Paez et al., 2017).

Roberts and Elmore (2017) reported evidence of hydrothermal alteration in the Woodford Shale in the Anadarko Basin in Oklahoma. This diagenetic study utilizing two cores found the following hydrothermal minerals: magnesite, norsethite, gorceixite, and potassium feldspar which were identified based on energy dispersive analysis. Other minerals that may be hydrothermal include sphalerite, chalcopyrite, witherite, saddle dolomite, apatite, and albite. These minerals are interpreted to have precipitated during middle-late diagenesis, mostly in mineralized fractures.

Methodology

The Core B sampled in this study contains a total of 179 ft (55 m) of Woodford Shale, with depths ranging from 3,317-3,496 ft (1,011-1,066 m), was oriented using the scribe method (Nelson et al., 1987). The core is vertical and the bedding is horizontal.

A total of 12 polished thin sections spanning the length of the core were made for petrographic methods. Diagenetic interpretations were made using a Zeiss AxioImager.Z1m petrographic microscope accompanied by AxioVision software for reflected and transmitted light imaging, and a Cambridge Image Technology LTD CLmk4 for cathodoluminescence (CL) microscopy to aid in phase identification and describe fluid-flow events. The thin sections as well as rock chips were examined using a FEI Quantam 250 Scanning Electron Microscope (SEM) with a Bruker Electron Dispersive Spectrometer (EDS) to further qualify phases and cross-cutting relationships. An x-ray computed tomography (XRCT) scan was obtained from the Nano Lab in the Mewbourne School of Petroleum and Geological Engineering on one 1” plug to characterize complex fracture networks. A Vickers M17 Research Microscope system adapted for reflected white light on slides immersed in oil at a magnification of 500x was used to obtain vitrinite and bitumen reflectance data following the American Society for Testing and Materials guidelines (ASTM, 2014). In addition to the vitrinite reflectance data, this bitumen reflectance data was used to calculate vitrinite reflectance equivalent (VRE) values for thermal maturity (Schoenherr et al., 2007; Landis & Castaño, 1994; Barker & Pawlewicz, 1986).

Thirty vertical, oriented plugs 1 in (2.5 cm) in diameter were taken from depths ranging the Woodford Shale section of Core B. A dual-blade water-cooled rock saw was

used to trim the plugs down to 0.87 in (2.2 cm) long specimens. A total of 3 specimens were subjected to alternating field (AF) demagnetization up to 120 mT in 10 mT increments, and 34 specimens underwent stepwise, thermal demagnetization in increments no greater than 20-50°C up to 500°C. The samples were baked with an ASC Scientific Thermal Demagnetizer, and the magnetization was measured using a 2G-Enterprises cryogenic magnetometer with a direct current superconducting quantum interference device in a magnetically shielded room. Demagnetization data was plotted on Zijderveld diagrams, from which magnetic components were found using principal component analysis (Kirschvink, 1980). Magnetic components with mean angles of deviation (MAD) less than 18^{o} were selected to calculate mean statistics (Fisher, 1953). Additionally, three specimens that had previously undergone AF demagnetization to remove any remanent magnetization were subjected to isothermal remanent magnetization (IRM) acquisition at room temperature using an ASC Scientific impulse magnetizer in order to characterize the magnetic mineralogy.

Results and Interpretations

Diagenesis

The stratigraphy of Core C is dominated by cherty and siliceous facies, with the least common facies being argillaceous and dolomitic. The lower section is characterized by siliceous and argillaceous facies with sparse grey, silty laminae. The grey laminae and the argillaceous facies decrease up section where cherty and siliceous facies that are either massive or contain faint dark grey laminae dominate. These siliceous and cherty facies continue to dominate in the upper portion of the core, with increasing amounts of

interbedded argillaceous facies and grey silty and dolomitic laminae. Fracturing and brecciation is common throughout the core and occurs primarily in the siliceous and cherty facies.

The Woodford Shale displays a complex paragenesis with evidence of multiple fracturing, brecciation, and fluid-flow events (Fig. 2-2). Events within the matrix and allochems occur primarily during earlier diagenesis while events associated with fracturing dominate later diagenesis.

Pyrite is found throughout the core as concretions, framboids, and disseminated in the matrix, and likely formed from the sulfate reduction process during early diagenesis (Schieber, 2011). The most common allochems present are radiolaria and tasmanites. During early diagenesis, allochems are often replaced by calcite and/or dolomite which is followed by replacement by silica (e.g., Schiber et al., 2000). Pyritization of allochems by euhedral crystals occurs after these events. Phosphate nodules common in the upper section of the core formed as a result of processes associated with compaction and lithification during early diagenesis (e.g., Murthy et al., 2004). Barite and silica are found filling pores within the nodules and are interpreted to have occurred during early diagenesis. Quartz overgrowths also occurred during early diagenesis.

The maturation of organic matter, illitization, and dolomitization occurred during late early-middle diagenesis. Euhedral albite crystals found in phosphate nodules are also interpreted as occurring during early-middle diagenesis.

Fracturing is dominantly vertical to sub-vertical in nature, although horizontal fractures do occur. There is evidence of multiple brecciation events throughout diagenesis. Mineralization within fractures is complex and often contains multiple

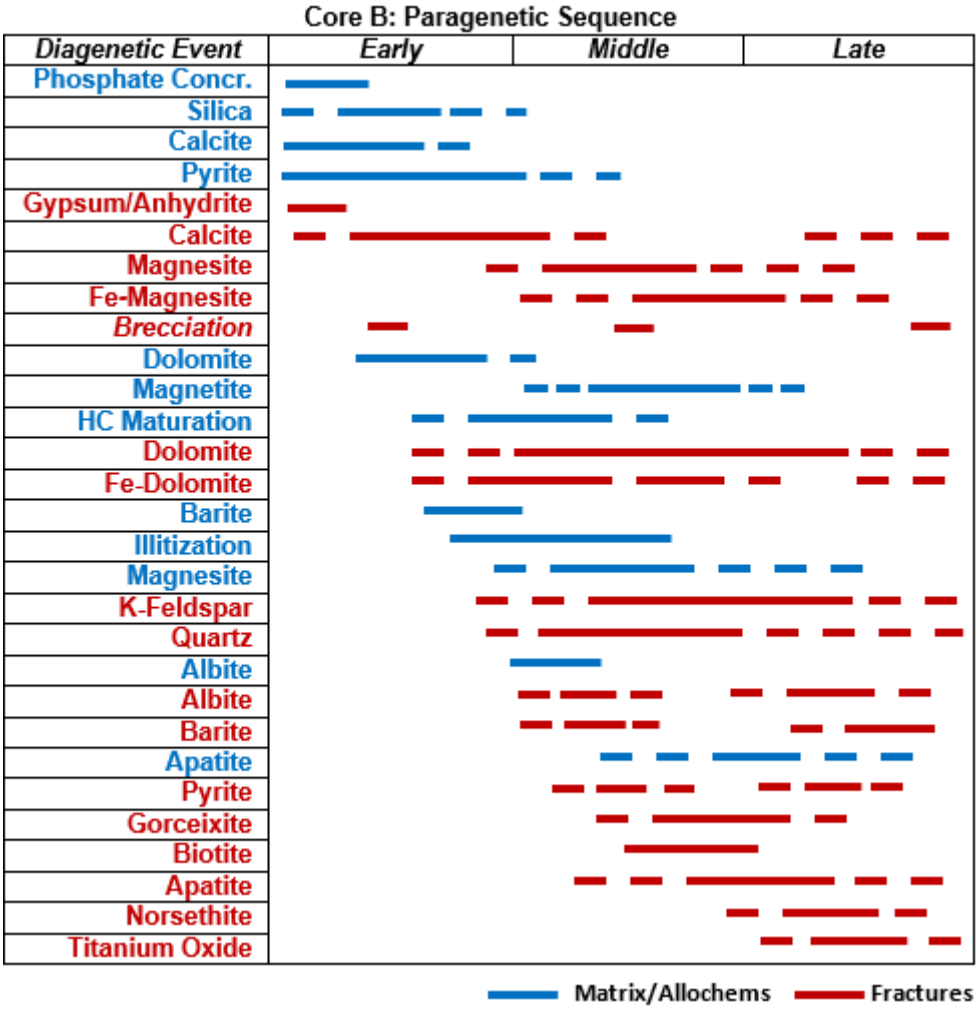

Figure 2-2. Paragenetic sequence for Core B. Events are listed from early to late. Timing is based on cross-cutting and textural relationships. Events in blue occur within the matrix and allochems, while events in red occur in the fracture fills. Dashed line refers to uncertainty in timing.

minerals (Fig. 2-2; Fig. 2-3a-f). Both dolomite and calcite precipitation occur in multiple fracture-filling events within early, middle, and late diagenetic stages (Fig. 2-3a,b,e,f).

The majority of minerals in fractures are interpreted as occurring during middle-late diagenesis, including potassium feldspar, albite, quartz, barite, norsethite ($BaMg[CO_3]_2$), pyrite, gorceixite ($BaAl_3(PO_4)(PO_3OH)(OH)_6$), apatite, biotite, and magnesite ($MgCO_3$) (Fig. 2-3a-f). Minerals such as norsethite (Fig. 2-3e), gorceixite (Fig. 2-3c,d), and magnesite (Fig. 2-3b,f) were identified based on energy dispersive analysis. Biotite occurs in a horizontal fracture-fill and is interpreted as forming during middle diagenesis. It occurs in association with and at the same time as potassium feldspar that is being altered to albite, along with pyrite, barite, apatite, and dolomite (Fig. 2-3a). A titanium oxide also found in this fracture is interpreted as occurring during late diagenesis based on cross-cutting relationships. Based on the occurrence of the feldspar in the fracture and its blocky crystal habit, it is interpreted as adularia (Deer et al., 1963). Megaquartz-filled fractures are common throughout the core (Fig. 2-3b,c,e). Magnesite is found in fractures, permeating the matrix, and around allochems (Fig. 2-3b,f).

The presence of magnetite is inferred from paleomagnetic analysis, and is interpreted as occurring during middle-early late diagenesis. Tabular aggregates of apatite crystals that occur in the matrix are interpreted as forming during middle-late diagenesis.

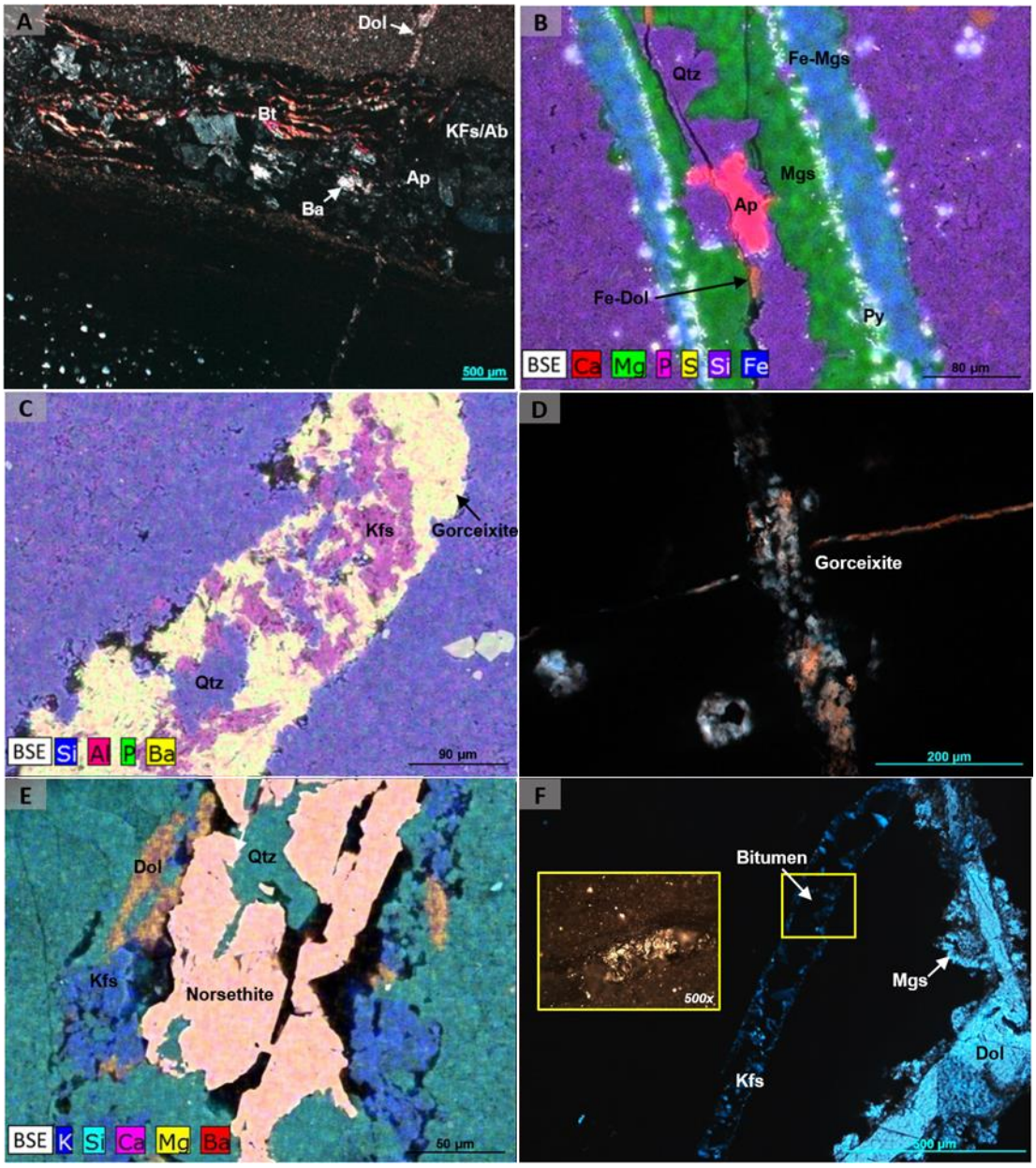

Figure 2-3. Diagenetic minerals and features within Core B. A) Photomicrograph under crossed polars (CPO) displaying a horizontal fracture filled with biotite and potassium feldspar being altered to albite, apatite, and barite. This fracture also contains the opaque minerals pyrite and a titanium oxide. The horizontal fracture is cut by a vertical dolomite-filled fracture. B) Backscatter SEM image (BSE) with elemental dispersive spectroscopy (EDS) overlay and the interpreted phases. The fracture contains Fe-magnesite (blue-green), pyrite (blue-yellow), magnesite (green), quartz (purple), apatite (red-pink), and Fe-dolomite (orange). C) BSE image with an EDS overlay displaying a fracture filled with gorceixite (yellow-green-pink), potassium feldspar (pink-blue), and quartz (blue). D) Photomicrograph in CPO of two cross-cutting fractures containing gorceixite. The round allochems in the southwest corner of the slide are silicified radiolaria,

one of which has been partially replaced by pyrite. E) BSE image with an EDS overlay and the interpreted phases. The fracture contains dolomite (orange), potassium feldspar (blue), norsethite (red-yellow), and quartz (cyan). F) Photomicrograph under CPO of one fracture containing dolomite and magnesite, and another containing potassium feldspar and pyrobitumen. The latter was used to obtain bitumen reflectance values used to calculate a vitrinite reflectance equivalent (VRE) value. This pyrobitumen is displayed as a reflected-light image highlighted by the yellow box. (Dol=dolomite, Bt=biotite, Ba=barite, Ap=apatite, Kfs=potassium feldspar, Ab=albite, Mgs=magnesite, Qtz=quartz, Py=pyrite)

Paleomagnetism

Thermal demagnetization reveals two magnetic components present in Core B (Fig. 2-4a-c). The first is a viscous remanent magnetization (VRM) held in unstable magnetic minerals. This is unblocked at low temperatures (NRM to ~175°C) with a north-northwesterly declination and a moderate-steep down inclination. The second is a characteristic remanent magnetization (ChRM) unblocked at higher temperatures (275-450°C) with a south-southeasterly declination and a shallow inclination that is interpreted to reside in magnetite. The ChRM is found in specimens spanning the length of the core, including those that are highly altered. On average, specimens containing the ChRM have more than double the magnetic intensity of those that do not. The ChRM is present in 24 of the 34 specimens thermally demagnetized. Although five of the remaining specimens contain what is interpreted as the ChRM, their MAD angles were unacceptable (>18°) and/or the directions were inconsistent with the ChRM direction. The remaining five specimens do not contain stable magnetizations. At temperatures higher than 450°C the magnetic intensity increases, likely due to the oxidation of pyrite. AF demagnetization isolated the ChRM from 20 - 120 mT with southeasterly declinations and moderate down inclinations. However, because of the possibility that the ChRM was partially

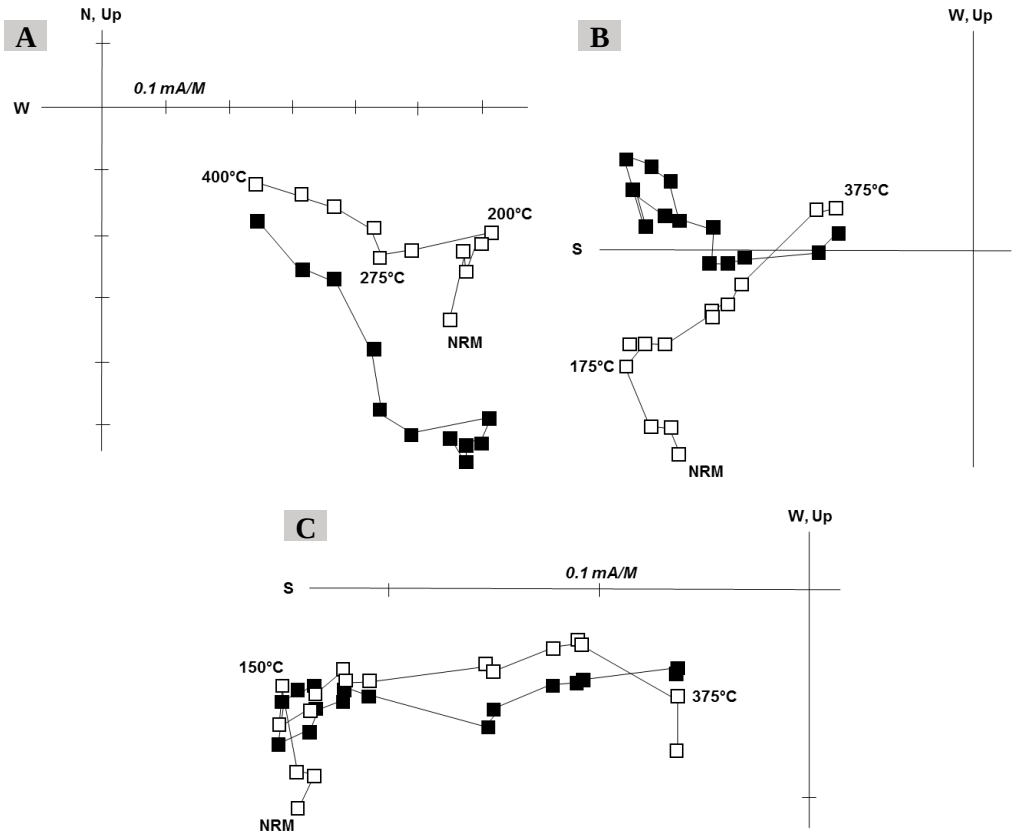

Figure 2-4. Thermal demagnetization data (a-c) displayed using Zijderveld plots. Closed squares represent the horizontal component of the magnetic field, while open squares represent the vertical component. The characteristic magnetization (ChRM) is the linear component decaying at the highest temperatures with south-southeasterly declinations and shallow inclinations. The unblocking temperatures for the ChRM components are the highest temperatures annotated on each figure.

contaminated by the modern component during AF demagnetization (McCabe et al., 1984) the specimen directions were not used to calculate the mean. A few specimens contain a possible third component which is unblocked at intermediate temperatures (175-275°C) with an easterly declination and a moderate-up inclination. Because it is poorly defined and was only found in a few specimens, a mean direction was not calculated. Isothermal remanent magnetization (IRM) acquisition was conducted to further characterize the magnetic mineralogy, however, results were inconclusive.

The ChRM specimen directions are well grouped on an equal area plot (Fig. 2-5). A virtual geomagnetic pole (VGP) obtained for the mean (Table 2-1) was plotted on an apparent polar wander path (APWP) for North America (Torsvik et al., 2012) and used to date the timing of the magnetizations (Fig. 2-6). The ChRM plots on the path at 250 ± 20 Ma, suggesting it is Late Permian in age.

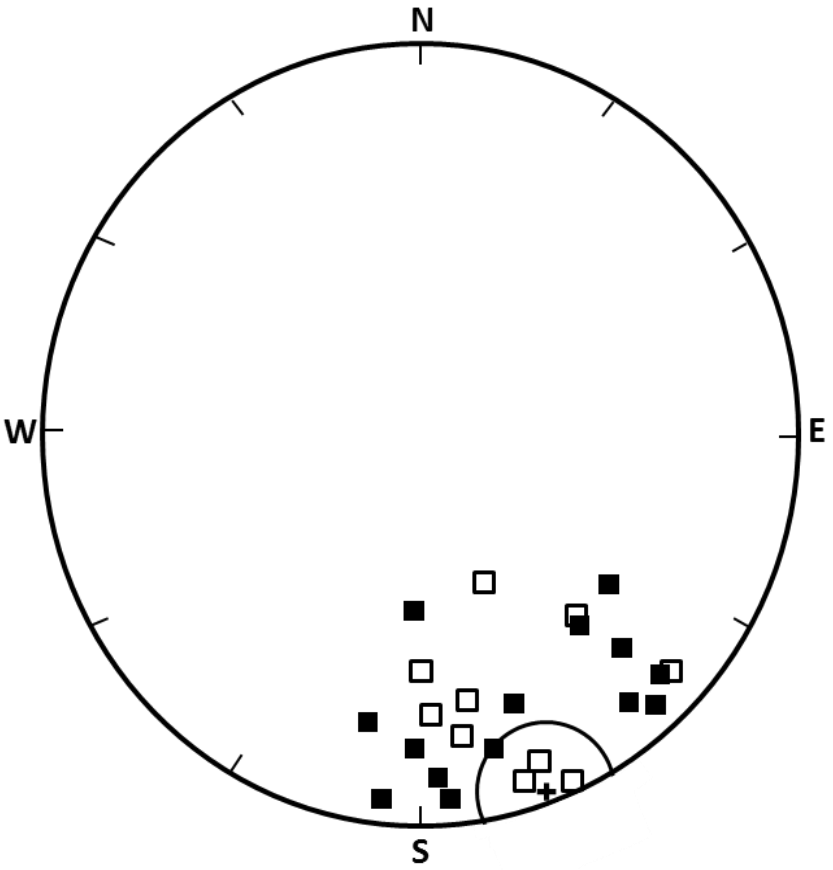

Figure 2-5. Fisher equal-area projection of the ChRM specimen directions. Declination is measured clockwise from north. Inclination is 0° at the edge of the circle and 90° at the center. Closed squares represent down inclinations; open squares represent up inclinations. The plus symbol is the mean direction and its surrounding circle is the α_{95} confidence limit.

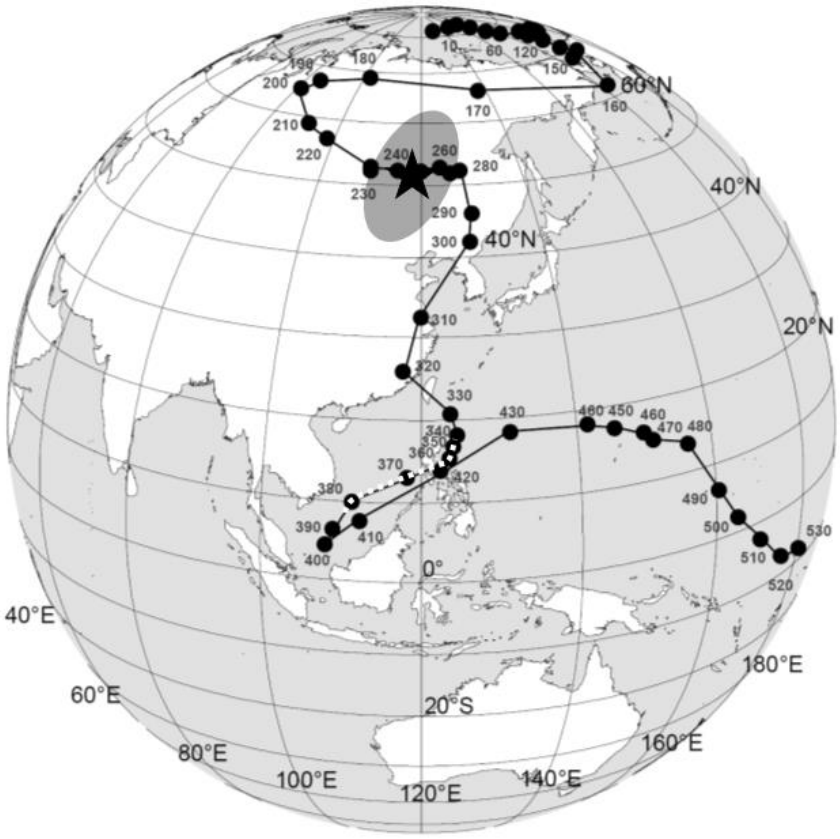

Figure 2-6. North American apparent polar wander path (APWP). The white dashed line along the path indicates the age of deposition for the Woodford Shale. The calculated virtual geomagnetic pole (VGP) for the ChRM is represented by the star, with the 95% confidence ellipse. The pole intersects the path at 250 ± 20 Ma, making it Late Permian in age. Modified from Torsvik and others (2012).

Table 2-1. Site mean and virtual geomagnetic pole (VGP) statistics for the characteristic remanent magnetization (ChRM).

Site Mean Statistics					*VGP*			
Dec	Inc	α_{95}	*k*	n/n_o	*Lat*	*Lon*	*dp*	*dm*
160.5°	1.1°	10.4°	9.08	24/29	51.0°N	115.7°E	5.2	10.4

Site Mean Statistics: Dec = declination; Inc = inclination; α_{95} = the radius of error about the site mean direction, within which there is a 95% probability that the true mean lies; k = precision parameter indicating relative dispersion about the mean direction; n/n_o = ratio of specimens used to specimens analyzed.
VGP Statistics: VGP (virtual geomagntic pole) = paleopole position calculated from the ChRM mean statistics; dp = length of VGP confidence ellipse along the site-to-pole great circle; dm = length of semi-axis of VGP confidence ellipse perpendicular to the site-to-pole great circle.

To test that the declination of the ChRM was not rotated in the core barrel, the ChRM was also dated using only the inclination (Appendix A). The core is vertical so this approach is valid. The inclination of the ChRM (1.1°) was compared to a graph displaying the expected inclination for the location of Core B. This dating approach resulted in an age of 285-245 Ma, or Early Permian to Middle Triassic in age. This is consistent with the age found using the declination information, therefore suggesting that the age obtained from the APWP is valid.

Discussion

A number of the minerals in the Woodford Shale suggest alteration by hydrothermal fluids, including magnesite, albite, norsethite (e.g., Bötcher, 2000; Steyn & Watson, 1967), apatite (e.g., Bouzari et al., 2016), gorceixite, biotite, and potassium feldspar. For the purposes of this study, hydrothermal fluids are defined here as "*aqueous solutions that are warm or hot relative to the surrounding environment*" (White, 1957),

which allows the term to be applied in diagenetic studies. Fluids at temperatures 5-10ºC higher than the host rock are considered to be significant (Machel & Lonnee, 2002; Stearns et al., 1935).Magnesite is known to form from the movement of warm magnesium-rich fluids that derived its magnesium from dolomite in underlying units (Shand, 2006). Albite can form at low temperatures but can also form from hydrothermal fluids (Kastner, 1971). Gorceixite has been tied to carbonaceous-argillic shales that have been altered by hydrothermal and volcanic activity (e.g., Migaszewski et al., 2007). Wang and others (2014) found biotite associated with gold ore of postcollisional magmatic hydrothermal origin in a black shale. Shelton and others (1986) linked quartz veinlets and potassium feldspar of the adularia variety to postcollisional hydrothermal alteration in the Womble Shale in the Ouachita Mountains in Arkansas. The abundance of quartz-filled fractures in Core B suggests the necessary pressure-temperature conditions were reached to cause the dissolution and precipitation of silica within a hydrothermal system (e.g., Okamoto et al., 2010).

The results from Roberts and Elmore (2017), which examined two Woodford Shale cores in the southeastern Anadarko Basin, are consistent with the interpretation that the Woodford Shale was locally altered by hydrothermal fluids. The Grady county core from that study contains almost all of the same hydrothermal minerals as Core B with the exception of biotite. Additionally, the Grady county core contains the hydrothermal minerals chalcopyrite, saddle dolomite, sphalerite, and witherite, which have not, as of yet, been identified in Core B. The McClain county core in the study by Roberts and Elmore (2017) contains significantly less hydrothermal alteration than that of the Grady county core and Core B, with the only hydrothermal mineral present being magnesite.

Thermal maturities across all three cores are consistent with these trends in hydrothermal alteration, with the Grady county core and Core B being the most thermally mature, and the McClain county core being the least thermally mature.

Based on unblocking temperatures, the ChRM is interpreted to reside in magnetite. Thermal maturity information was obtained from vitrinite in the matrix and pyrobitumen found in fractures (Fig. 2-3f). Six vitrinite reflectance values were obtained having an average R_o value of 1.82%, equating to a maximum heating temperature of approximately 230°C (Barker & Pawlewicz, 1986). Bitumen reflectance values were converted into vitrinite reflectance equivalent (VRE) values following equations provided by Schoenherr and others (2007) and Landis and Castaño (1994), yielding VRE values of 1.47% and 1.57%, respectively. This equates to maximum heating temperature of approximately 210°C (Barker & Pawlewicz, 1986). Alteration temperatures this high could have exerted an influence on the ChRM (e.g., Pullaiah et al., 1978; Kent, 1985). Therefore, this secondary magnetization is interpreted as either a CRM that formed from the chemical growth of magnetite or a thermochemical remanent magnetization (TCRM) from the combination of magnetite growth and thermal resetting of the magnetization. Because of the high thermal maturity and the fact that specimens with the CRM/TCRM contain extensive hydrothermal alteration, the magnetite identified from the magnetic analysis is interpreted to have formed from hydrothermal fluids.

While Core B contains hydrothermal minerals, it is important to note that the elements found in these minerals could have been sourced internally from the shale. Many of these minerals have also been found in rock that is not reported as hydrothermally altered, such as norsethite (Mrose et al, 1961) and albite (Kastner, 1971; Poole et al.,

2014). However, it is unlikely that the source of heat came from the shale. It is also not clear that the fluids could have leached all of the elements from the shale. The abundance of hydrothermal minerals and the temperature information suggests that a hydrothermal source is a valid interpretation. This implies that the shale may have evolved from a closed system during early diagenesis to a system open to external fluids during late diagenesis.

Hydrothermal alteration in shales has important implications as it pertains to oil and gas exploration in unconventional shale reservoirs. The exposure of the reservoir to high temperatures by these fluids can lead to cracking of hydrocarbons and possibly result in an overly thermally-mature reservoir, at least locally. This process can also lead to the formation of gas and subsequently porosity in organic matter (Jarvie et al., 2007). While the warm fluids could have created porosity and permeability through dissolution, the presence of minerals such as magnesite permeating the matrix suggests that more porosity could have been destroyed than created. Additionally, various hydrothermal minerals introduced to the shale can either inhibit or enhance brittle behavior, thus affecting the unit's susceptibility to hydraulic fracturing. For example, carbonate minerals such as magnesite and norsethite are believed to increase the brittleness of the rock (e.g., Jin et al., 2015). Hydrothermal silicate minerals such a feldspar and quartz also contribute to the brittleness (Jin et al., 2015). Natural fractures can influence hydraulic fracturing (e.g., Olson & Dahi-Taleghani, 2010) and the fact that some of the hydrothermal minerals permeate from the fractures into the matrix could add to the brittleness. Ultimately, hydrothermal alteration of shale can introduce uncertainty during the exploration process.

Other studies conducted in southern Oklahoma and the Ouachita Mountains suggest that the rocks in the region have been altered by a hydrothermal event in the Late

Permian. For example, Shelton and others (1986) found Ba-rich adularia in the Womble Shale (Late Ordovician) in the Ouachita Mountains associated with post-folding quartz veinlets. Based on the fluid inclusion data from the adularia and quartz veins which yielded a maximum formation temperature of 300°C, both minerals formed from hydrothermal fluids. K-Ar dating of the adularia yielded an age of formation of 262 ± 10 Ma (Late Permian). The mechanism proposed for this fluid-flow event was post-folding faulting in the Ouachita Mountains that accessed a reservoir of hot fluids, subsequently resulting in hydrothermal alteration. It was suggested that this hydrothermal alteration in the Womble is linked to the widespread fluid expulsion event in the Late Paleozoic from the Appalachian-Ouachita orogeny that resulted in the Mississippi Valley-type (MVT) Pb-Zn-Ba deposits in the Mid-Continent.

Additionally, Elmore and others (1993) found alteration by warm fluids in and around veins in the Viola Limestone in the Arbuckle Mountains. Hematite alteration around veins containing calcite and MVT oxides and sulfides was dated using paleomagnetic methods to the Late Permian. Sr isotope and fluid inclusion data indicate the vein mineralization was attributed to the migration of warm, basinal fluids with elevated $^{87}Sr/^{86}Sr$ values through fractures and into the surrounding host-rock.

The coincidence of these three events at about the same age suggests a common origin. The most likely possibility for this is the migration of hydrothermal fluids as a result of faulting. Sharp (1978) proposed that faulting in the Ouachita Mountains and Arkoma Basin could have accessed rock containing hot fluids and provided conduits for these fluids to deposit MVT mineralization across northern Arkansas and southeastern Missouri. This origin was also suggested by Shelton

and others (1986) for the Late Permian hydrothermal mineralization found in the Womble Shale in the Ouachita Mountains. Knowing that Core B cuts through a fault about 2,000 ft (~600 m) above the Woodford formation and that faulting is common in the area (Marsh & Holland, 2016) further supports this reasoning. More work is necessary to determine how widespread this hydrothermal event was.

Conclusions

The Woodford Shale displays significant alteration through multiple fracturing, brecciation, and mineralization events. Numerous diagenetic minerals largely found in fractures, such as norsethite, potassium feldspar, albite, gorceixite, biotite, and quartz, and occasionally in the matrix, including magnesite and apatite, suggest that the Woodford Shale has been altered by hydrothermal fluids. The R_o values and VRE values obtained from the reflectance of pyrobitumen found filling fractures yields a maximum thermal alteration of approximately 210-240°C. Paleomagnetic results indicate a CRM or TCRM residing in magnetite that formed in the Late Permian. Core B's high thermal maturities and significant quantities of hydrothermal minerals suggest that the Woodford Shale was altered by externally derived hydrothermal fluids in the Late Permian. This has significant implications pertaining to the exploitation of the unit as an unconventional reservoir, such as high thermal maturity and decreased porosity and permeability, and also implies that the Woodford Shale evolved into an open system in the Late Permian. The agreement in timing with other studies which report hydrothermal alteration in southern Oklahoma and eastern Arkansas at about the same time (e.g., Elmore et al.,

1993; Shelton et al., 1986) suggest there may have been a widespread postcollisional fluid-flow event in the Late Paleozoic.

Summary of Research

All three cores from Chapters 1 and 2 contain many of the same diagenetic events within the matrix and allochems. However, the norsethite in the matrix of Core C, the barite in the matrix of Core B, the ferroan dolomite overgrowths on detrital dolomite grains in Core A, the apatite replacing allochems in Core A, and the magnetite found in Cores B and C, have yet to have been identified in the other cores. Additionally, the fracture diagenesis varies between cores. All three cores contain dolomite, calcite, pyrite, magnesite, and quartz in fractures. With the exception of the presence of chert in the fractures, which Cores B and C do not contain, Core A stands out due to its much more simplistic diagenesis. Cores B and C are quite similar in their fracture diagenesis with a few exceptions - Core B contains biotite, and Core C contains chalcopyrite, sphalerite, witherite, and saddle dolomite.

The hydrothermal alteration in each core varies, and this variation correlates to the thermal maturity of each Core. Core A is the least mature with a 0.80% VR_o (~125°C) and displays the lowest amount of hydrothermal minerals, with only magnesite and apatite present. Core C has an intermediate thermal maturity relative to the other cores with an approximately 1.5% VR_o (~210°C), and contains the hydrothermal minerals norsethite, magnesite, witherite, saddle dolomite, potassium feldspar, albite, gorceixite, chalcopyrite, sphalerite, and apatite. Core B is the most thermally mature with an approximately 1.82% VR_o (~230°C), and contains the hydrothermal minerals norsethite, magnesite, biotite, potassium feldspar, albite, apatite, and gorceixite. Additionally, Core B contains a significant amount of quartz veinlets which are commonly found in hydrothermal systems. It is important to note that although the elements found in these

minerals could have been intrinsically present in the shale, an external hydrothermal source is necessary to explain the higher thermal maturities such as displayed in Core B. It is also not clear that fluids could have leached all of the elements from within the shale alone. This suggests that the shale may have evolved from a closed system during early diagenesis to a system open to external fluids during late diagenesis.

The paleomagnetic dating of Core B revealed a characteristic remanent magnetization (ChRM) residing in magnetite dated to the Late Permian. Based off of the high thermal maturity of Core B and the level of hydrothermal alteration, the ChRM is interpreted as either a chemical remanent magnetization (CRM) that formed from the chemical growth of magnetite or a thermochemical remanent magnetization (TCRM) that formed from the combination of magnetite growth and the thermal resetting of the magnetization. The CRM/TCRM is interpreted as originating from a hydrothermal fluid-flow event.

Other studies conducted in southern Oklahoma and the Ouachita Mountains suggest that the rocks in the region have been altered by a hydrothermal event in the Late Permian. For example, Shelton and others (1986) found Ba-rich adularia in the Womble Shale (Late Ordovician) in the Ouachita Mountains associated with post-folding quartz veinlets. Based on the fluid inclusion data from the adularia and quartz veins which yielded a maximum formation temperature of 300°C, both minerals formed from hydrothermal fluids. K-Ar dating of the adularia yielded an age of formation of 262 ± 10 Ma (Late Permian). Additionally, Elmore and others (1993) found alteration by warm fluids in and around veins in the Viola Limestone in the Arbuckle Mountains. Hematite alteration around veins containing calcite and Mississippi Valley-type (MVT) oxides and

sulfides was dated using paleomagnetic methods to the Late Permian. Sr isotope and fluid inclusion data indicate the vein mineralization was attributed to the migration of warm, basinal fluids with elevated $^{87}Sr/^{86}Sr$ values through fractures and into the surrounding host-rock. The coincidence of these three events at about the same age suggests a common origin. One possibility is the migration of hydrothermal fluids as a result of faulting that accessed reservoir(s) of warm fluids and facilitated their movement through fault and fracture networks (Sharp, 1978; Shelton et al., 1986).

Future Work

Fluid inclusion work will be done in order to further characterize the hydrothermal fluids that altered the Woodford Shale. Additional petrographic analysis of the cores using newly acquired thin sections will greatly aid in refining their paragenetic sequences. The acquisition of rock magnetic data will be used to further support the interpretation that the magnetization found in Core B resides in magnetite.

References

American Society for Testing and Materials (ASTM), 2014, Standard test method for microscopical determination of the reflectance of vitrinite dispersed in sedimentary rocks: West Conshohocken, PA, ASTM International, Annual book of ASTM standards: Petroleum products, lubricants, and fossil fuels; Gaseous fuels; coal and coke, **5.06**, **D7708-14**, 823-830.

Barker, C.E., and M.J. Pawlewicz, 1986, The correlation of vitrinite reflectance with maximum temperature in humic organic matter: Paleogeothermics: Springer-Verlag, Lecture Notes in Earth Sciences, **5**, 79-93, doi: 10.1007/BFb0012103

Berner, R.A., J.W. Leeuw, B. Spiro, D.G. Murchison, and G. Eglinton, 1985, Sulphate reduction, organic matter decomposition and pyrite formation [and discussion]: Philosophical Transactions of the Royal Society of London. Series A, Mathematical and Physical Sciences, **315**, 25-38, doi: 10.1098/rsta.1985.0027

Berryman, J., 2013, Timing and paragenesis of the calcite fracture fill in the Woodford Shale: Shale Shaker, **(Jul-Aug)**, 40-53.

Bethke, C.M., and S. Marshak, 1990, Brine migration across North America - the plate tectonics of groundwater: Annual Review of Earth and Planetary Sciences, **18**, 228-315, doi: 10.1146/annurev.ea.18.050190.001443

Bjorlykke, K., and J. Jahren, 2012, Open or closed geochemical systems during diagenesis in sedimentary basins: Constraints on mass transfer during diagenesis and the prediction of porosity in sandstone and carbonate reservoirs: American Association of Petroleum Geologists Bulletin, **96**, 2193-2214, doi: 10.1306/04301211139

Blumstein, A., R.D. Elmore, and M. Engel, 2004, Paleomagnetic dating of burial diagenesis in Mississippian carbonates, Utah: Journal of Geophysical Research, **109**, 2156-2202, doi: 10.1029/2003JB002698

Bötcher, M., 2000, Stable isotope fractionation during experimental formation of norsethite (BaMg[CO3]2): A mineral analogue of dolomite: Aquatic Geochemistry, **6**, 201212, doi: 10.1023/A:1009646805933

Bouzari, F.B., C.J.R. Hart, T. Bissig, and S. Barker, 2016, Hydrothermal alteration revealed by apatite luminescence and chemistry: A potential indicator mineral for exploring covered porphyry copper deposits: Economic Geology, **111**, 1397-1410, doi: 10.2113/econgeo.111.6.1397

Boyd, D.T., 2008, Stratigraphic guide to Oklahoma oil and gas reservoirs: Oklahoma Geological Survey Special Publications.

Burruss, R.C., and J.R. Hatch, 1989, Geochemistry of oils and hydrocarbon source rocks, greater Anadarko basin: evidence for multiple sources of oils and long distance oil migration: Oklahoma Geological Survey Circular, **90**, 53-64.

Cardott, B J., 2013, Woodford Shale: From hydrocarbon source rock to reservoir: AAPG Search and Discovery Article #50817.

Cardott, B.J. and M.W. Lambert, 1985, Thermal maturation by vitrinite reflectance of Woodford Shale, Anadarko basin, Oklahoma: AAPG Bulletin, **69**, 1982-1998.

Cardott, B.J., 2012, Thermal maturity of Woodford Shale gas and oil plays, Oklahoma, USA: International Journal of Coal Geology, **103**, 109-119, doi: 10.1016/j.coal.2012.06.004

Chalmers, G. R., R.M. Bustin, and M. Power, 2012, Characterization of gas shale pore systems by porosimetry, pycnometry, surface area, and field emission scanning electron microscopy/transmission electron microscopy image analyses: Examples from the Barnett, Woodford, Haynesville, Marcellus, and Doig units: AAPG Bulletin, **96**, 1099–1119, doi: 10.1306/10171111052

Chamberlain, S.C., W.P. Dossert, and D.I. Siegel, 1986, A new paragenesis and new localities for witherite: Canadian Mineralogist, **24**, 79-90.

Cobbold, P. R., A. Zanella, N. Rodrigues, and H. Løseth, 2013, Bedding-parallel fibrous veins (beef and cone-in-cone): Worldwide occurrence and possible significance in terms of fluid overpressure, hydrocarbon generation and mineralization: Marine and Petroleum Geology, **43**, 1–20, doi:10.1016/j.marpetgeo.2013.01.010

Coffman, J.D., M.C. Gilbert, and D.A. McConnell, 1986, An interpretation of the crustal structure of the Southern Oklahoma Aulacogen satisfying gravity data: Oklahoma Geological Survey Guidebook, **23**, 1-10.

Deer, W.A., R.A Howie, and J. Zussman, 1963, Rock-Forming Minerals: Framework Silicates: Longmans, Green & Co., London, **4**.

Dehandschutter, B., S. Vandycke, M. Sintubin, N. Vandenberghe, and L. Wouters, 2005, Brittle fractures and ductile shear bands in argillaceous sediments: inferences from Oligocene Boom Clay (Belgium): Journal of Structural Geology, **27**, 1095–1112, doi:10.1016/j.jsg.2004.08.014

Elmore, R., A. Muxworthy, and M. Aldana, 2012, Remagnetization and chemical alteration of sedimentary rocks: Geological Society, London, Special Publications, **371**, 1-21, doi: 10.1144/SP371.15

Elmore, R.D., D. London, D. Bagley, and D. Fruit, 1993, Remagnetization by basinal fluids: Testing the hypothesis in the Viola Limestone, Southern Oklahoma: Journal of Geophysical Research, **98**, 6237-6254, doi: 10.1029/92JB02577

Elmore, R.D., G.W. Heij, and A.K. Wickard, A.K., 2016, Paragenesis of mineralized fractures and diagenesis of prominent North American shales: The Sedimentary Record: SEPM, **14**, 4-10, doi: 10.2110/sedred.2016.4

Elmore, R.D., J. Haynes, S. Farzaneh, and S. Anzaldua, 2015, Integrated diagenetic and paleomagnetic study of the Mississippian Limestone, north central Oklahoma: AAPG Search and Discovery Article # 51163

Fisher, R.A., 1953, Dispersion on a sphere: Geophysical Journal of the Royal Astronomical Society, **217**, 295–305, doi: 10.1098/rspa.1953.0064

Gale, J. F. W., S.E. Laubach, J.E. Olson, P. Eichhuble, and A. Fall, 2014, Natural Fractures in shale: A review and new observations. AAPG Bulletin, **98**, 2165–2216. doi:10.1306/08121413151

Goldstein, R.H. and B.D. King, 2014, Impact of hydrothermal fluid flow on Mississippian reservoir properties, southern Midcontinent: Unconventional Resources Technology Conference (URTeC), doi: 10.15530/urtec-2014-1934915

González-Muñoz, M.T., B. Fernández-Luque, F. Martínez-Ruiz, K.B. Chekroun, J.M.Arias, M. Rodríguez-Gallego, M. Martínez-Cañamero, C. de Linares, and A. Paytan, 2003, Precipitation of Barite by Myxococcus xanthus: Possible Implications for the Biogeochemical Cycle of Barium: Applied and Environmental Microbiology, **69**, 5722-5725, doi: 10.1128/AEM.69.9.5722-5725.2003

Heij, G., J. Roberts, A.K. Steullet, and D. Dennie, 2016, Spatial-temporial boundaries of shale diagenesis inferred from magnetic fabrics and paleomagnetism: AAPG Search and Discovery Article #90283

Infante-Paez, L., L. Cardona, B. Mccullough, and R. Slatt, 2017, Seismic analysis of paleotopography and stratigraphic controls on total organic carbon: Rich sweet spot distribution in the Woodford Shale, Oklahoma, USA: Interpretation, **5**, T33-T47, doi: 10.1190/INT-2015-0151.1

Jarvie, D. M., R. J. Hill, T. E. Ruble, and R. M. Pollastro, 2007, Unconventional shale-gas systems: The Mississippian Barnett Shale of North-Central Texas as one model for thermogenic shale-gas assessment: AAPG Bulletin, **91**, 475–499, doi: 10.1306/12190606068

Jin, X., S.N. Shah, J.C. Roegiers, and B. Zhang, 2015, An integrated petrophysics and geomechanics approach for fracability evaluation in shale reservoirs: Society of Petroleum Engineers Journal, **20**, 518-526, doi:10.2118/168589-pa

Johnson, K. S., 1989, Geologic evolution of the Anadarko Basin: Oklahoma Geological Survey Circular, **90**, 3-12.

Kastner, M., 1971, Authigenic feldspars in carbonate rocks: American Mineralogist, **56**, 1403-1442.

Katz, B., R.D. Elmore, M.H. Engel, M. Cogoini, and S. Ferry, 2000, Associations between burial diagenesis of smectite, chemical remagnetization, and magnetite authigenesis in the Vocontian trough, SE France: Journal of Geophysical Research: Solid Earth, **105**, 851-868, doi: 10.1029/1999JB900309

Kent, D.V., 1985, Thermoviscous remagnetization in some Appalachian limestones: Geophysical Research Letters, **12**, 805–808, doi: 10.1029/GL012i012p00805

Kirkland, D.W., R.E. Denison, D.M. Summers, and J.R. Gormly, 1992, Geology and organic geochemistry of the Woodford Shale in the Criner Hills and western Arbuckle Mountains, Oklahoma: Oklahoma Geological Survey Circular, **93**, 38-69.

Kirschvink, J.L., 1980, The least squares line and plane and the analysis of paleomagnetic data: Geophysics Journal Royal Astronomical Society, **62**, 699-718, doi: 10.1111/j.1365-246X.1980.tb02601.x

Land, L.S., L.E. Mack, K.L. Milliken, and F.L. Lynch, 1997, Burial diagenesis of argillaceous sediment, south Texas Gulf of Mexico sedimentary basin: A reexamination: Geological Society of America Bulletin, **109**, 2–15, doi: 10.1130/0016-7606(1997)109%3C0002:BDOASS%3E2.3.CO;2

Landis, C.R., and J.R. Castaño, 1994, Maturation and bulk chemical properties of a suite of solid hydrocarbons: Organic Geochemistry, **22**, 137-149, doi: 10.1016/0146-6380(95)90013-6

Laughrey, C. D. and P.F. Purrazzella, 2016, Petroleum geochemistry and mudstone diagenesis of the Woodford Shale, Anadarko Basin, USA - An integrated approach: AAPG Datapages/Search and Discovery Article #90283.

Lavoie D, G. Chi, P. Brennan-Alpert, A. Desrochers, and R. Bertrand, 2005, Hydrothermal dolomitization in the Lower Ordovician Romaine Formation of the Anticosti Basin: significance for hydrocarbon exploration: Bulletin of Canadian Petroleum Geology, **53**, 454-471, doi: 10.2113/53.4.454

Leach, D., and E. Rowan, 1986, Genetic link between Ouachita foldbelt tectonism and the Mississippi Valley–type lead-zinc deposits of the Ozarks: Geology, **14**, 931-935, doi: 10.1130/0091-7613(1986)14%3C931:GLBOFT%3E2.0.CO;2

Machel, H. G., and J. Lonnee, 2002, Hydrothermal dolomite—a product of poor definition and imagination.: Sedimentary Geology, **152**, 163–171, doi:10.1016/s0037-0738(02)00259-2

Maher, H., K. Ogata, and A. Braathen, 2016, Cone-in-cone and beef mineralization associated with Triassic growth basin faulting and shallow shale diagenesis,

Edgeøya, Svalbard: Geological Magazine, 1-16, doi:10.1017/S0016756815000886

Mann, E., 2014, Stratigraphic Study of Organic-rich Microfacies of the Woodford Shale, Anadarko Basin, Oklahoma: M.S. thesis, University of Oklahoma.

Marsh, S., and A. Holland, 2016, Comprehensive Fault Database and Interpretive Fault Map of Oklahoma: Oklahoma Geological Survey, Open-File Report (OF2-2016).

McCabe, C., R. Van der Voo, and M.M. Ballard, 1984, Late Paleozoic remagnetization of the Trenton Limestone: Geophysical Research Letters, American Geophysical Union, **11**, 979-982, doi: 10.1029/GL011i010p00979

Miceli Romero, A. and R.P. Philp, 2012, Organic geochemistry of the Woodford Shale, southeastern Oklahoma; how variable can shales be?: AAPG Bulletin, **96**, 493–517, doi: 10.1306/08101110194

Migaszewski, Z., E.Starnawska, and A. Gałuszka, 2007, Gorceixite from the Upper Cambrian Rocks of the podwiśniówka Mine Pit, Holy Cross Mountains (South Central Poland): Mineralogia, **38**, 171-184, doi: 10.2478/v10002-007-0025-6

Milliken, K. L., Esch,, W. L. , Reed, R. M., Zhang T., 2012, Grain assemblages and strong diagenetic overprinting in siliceous mudrocks, Barnett Shale (Mississippian), Fort Worth Basin, Texas, U.S.A.: AAPG Bulletin, **96**, 1553-1578, doi:10.1306/12011111129

Misch, D., F. Mendez-Martin, G. Hawranek, P. Onuk, D. Gross, and R.F. Sachsenhofer, 2016, SEM and FIB-SEM investigations on potential gas shales in the Dnieper-Donets Basin (Ukraine): Pore space evolution in organic matter during thermal maturation: IOP Conference Series: Materials Science and Engineering,**109,** 1-13, doi: 10.1088/1757-899X/109/1/012010

Mrose, M.E., E.C.T. Chao, J.J. Fahey, and C. Milton, 1961, Norsethite, BaMg(CO3)2, a new mineral from the Green River Formation, Wyoming. Amer. Mineral., **46**, 420–429.

Murthy, R., D. Kidder, R. Mapes, and R. Hannigan, 2004, Rare-earth element chemistry of Mississippian-age phosphate nodules in the Fayetteville Shale of Oklahoma and Arkansas: Environmental Geosciences, **11**, 99-111, doi: 10.1306/eg.01080403018

Nelson, R. A., L.C. Lenox, and B.J. Ward, 1987, Oriented core: It's use, error, and uncertainty: AAPG Bulletin, **71**, 357-367.

Northcutt, R.A. and J.A. Campbell, 1998, Geologic Provinces of Oklahoma: Basement Tectonics, **12**, 29-37.

Okamoto, A., H. Saishu, N. Hirano, and N. Tsuchiya, 2010, Mineralogical and textural variation of silica minerals in hydrothermal flow-through experiments: Implications for quartz vein formation: Geochimica et Cosmochimica Acta, **74**, 3692-3706, doi: 10.1016/j.gca.2010.03.031

Olson, J. and A. Dahi-Taleghani, 2010, The influence of natural fractures on hydraulic fracture propagation: AAPG Search and Discovery Article #40583.

Perry, Jr., W. J., 1989, Tectonic Evolution of the Anadarko Basin Region, Oklahoma U.S.: U.S. Geological Survey Bulletin, **1866-A**.

Pevear, D. R., 1999, Illite and hydrocarbon exploration: Proceedings of the National Academy of Sciences, **96**, 3440–3446, doi:10.1073/pnas.96.7.3440

Poole, S., 2014, Quantitative Mineralogy and Distributions of Minerals of the Green River Formation, Piceance Creek Basin, Western Colorado: M.S. thesis, Colorado School of Mines.

Pullaiah, G., Irving, E., Buchan, K.L., and Dunlop, D.J., 1975, Magnetization changes caused by burial and uplift: Earth and Planetary Science Letters, **28**, p. 133-143, doi: 10.1016/0012-821X(75)90221-6

Robbins, S.L. and G.R. Keller, 1992, Complete bouguer and isostatic residual gravity maps of the Anadarko Basin, Wichita Mountains, and surrounding areas, Oklahoma, Kansas, Texas, and Colorado: U.S. Geological Survey Bulletin, **1866-G**, G1-G11.

Roberts, J., R.D. Elmore, 2017, A diagenetic study of the Woodford Shale in the Anadarko Basin, Oklahoma, U.S.A.: Interpretation (Submitted).

Schieber, J., 2011, Iron Sulfide Formation: Encyclopedia of Geobiology, 486-502, doi: 10.1007/978-1-4020-9212-1_118

Schieber, J., D. Krinsley, and L. Riciputi, 2000, Diagenetic origin of quartz silt in mudstones and implications for silica cycling: Nature, **406**, 981-985, doi: 10.1038/35023143

Schoenherr, J., R. Littke, J.L. Urai, P.A. Kukla, and Z. Rawahi, 2007, Polyphase thermal evolution in the Infra-Cambrian Ara Group (South Oman Salt Basin) as deduced by maturity of solid reservoir bitumen: Organic Geochemistry, **38**, 1293-1318, doi: 10.1016/j.orggeochem.2007.03.010

Selleck, B., 2014, Geochemistry and sulfide mineral paragenesis in Marcellus subgroup and Utica formation gas shale intervals: Geological Society of America: Northeastern Section 49th Annual Meeting Abstract, Paper No. 53-7.

Shand, M.A., 2006, Formation and occurrence of magnesite and brucite, in The Chemistry and Technology of Magnesia. John Wiley & Sons, Inc. doi: 10.1002/0471980579.ch2

Sharp, J.M., Jr., 1978, Energy and momentum transport model of the Ouachita Basin and its possible impact on formation of economic mineral deposits: Economic Geology, **73**, 1057-1068.

Shelton, K.L., J.M. Reader, L.M. Ross, G.W. Viele, and D.E. Siedeman, 1986, Ba-rich adularia from the Ouachita Mountains, Arkansas—Implications for a post-collisional hydrothermal system: American Mineralogy, **71**, 916–923.

Shermin, G., G. Garven, 1989, Tectonically induced transient groundwater flow in foreland basin: in Origin and Evolution of Sedimentary Basins and their Energy and Mineral Resources: American Geophysical Union, 145-157, doi: 10.1029/GM048p0145

Slatt, R.M., & N.D. Rodriguez, 2012, Comparative sequence stratigraphy and organic geochemistry of gas shales: Commonality or coincidence?: Journal of Natural Gas Science and Engineering, **8**, 68-84, doi: 10.1016/j.jngse.2012.01.008

Stearns, N.D., H.T. Stearns, and G.A. Waring, 1935, Thermal springs in the United States: United States Geological Survey Water Supply Paper, **679-B**, 59-191.

Steyn, J.G.D. and M.D. Watson, 1967, Notes on a new occurrence of norsethite, BaMg(CO3)2: The American Mineralogist, **52**, 1770-1775.

Torsvik, T.H., R. Van der Voo, U. Preeden, C. M. Niocaill, B. Steinberger, P.V. Doubrovine, Douwe J.J. Van Hinsbergen, M. Domeier, C. Gaina, E. Tohver, J.G. Meert, Phil J.A. McCausland, L. Robin M. Cocks, 2012, Phanerozoic Polar Wander, Palaeogeography and Dynamics: Earth-Science Reviews, **114**, 325-68, doi: 10.1016/j.earscirev.2012.06.007

Turner, B., J. Tréanton, & R.M. Slatt, 2016, The use of chemostratigraphy to refine ambiguous sequence stratigraphic correlations in marine mudrocks. An example from the Woodford Shale, Oklahoma, USA: Journal of the Geological Society, **173**, 854-868, doi: 10.1144/jgs2015-125

Wang, J., J. Liu, R. Peng, Z. Liu, B. Zhao, Z. Li, Y. Wang, and C. Liu, 2014, Gold mineralization in Proterozoic black shales: Example from the Haoyaoerhudong gold deposit, northern margin of the North China Craton: Ore Geology Reviews, **63**, 150-159, doi: 10.1016/j.oregeorev.2014.05.001

White, D.E., 1957, Thermal waters of volcanic origin: Geological Society of America Bulletin, **68**, 1637 – 1658, doi: 10.1130/00167606(1957)68[1637:twovo]2.0.co;2

Williams, G., 2015, Hydrothermal alteration of Britain's oldest palaeosols: Saddle dolomite and smectite at the Lewisian-Torridon Group (early Neoproterozoic)

unconformity, NW Scotland: Scottish Journal of Geology, **51**, 63-68, doi: 10.1144/sjg2014-014

Wu, K., and J.E. Olson, 2014, Mechanics analysis of interaction between hydraulic and naturalfractures in shale reservoirs: Proceedings of the 2nd Unconventional Resources Technology Conference, doi: 10.15530/urtec-2014-1922946

Appendix A: Expected Inclination Plot (Core B)

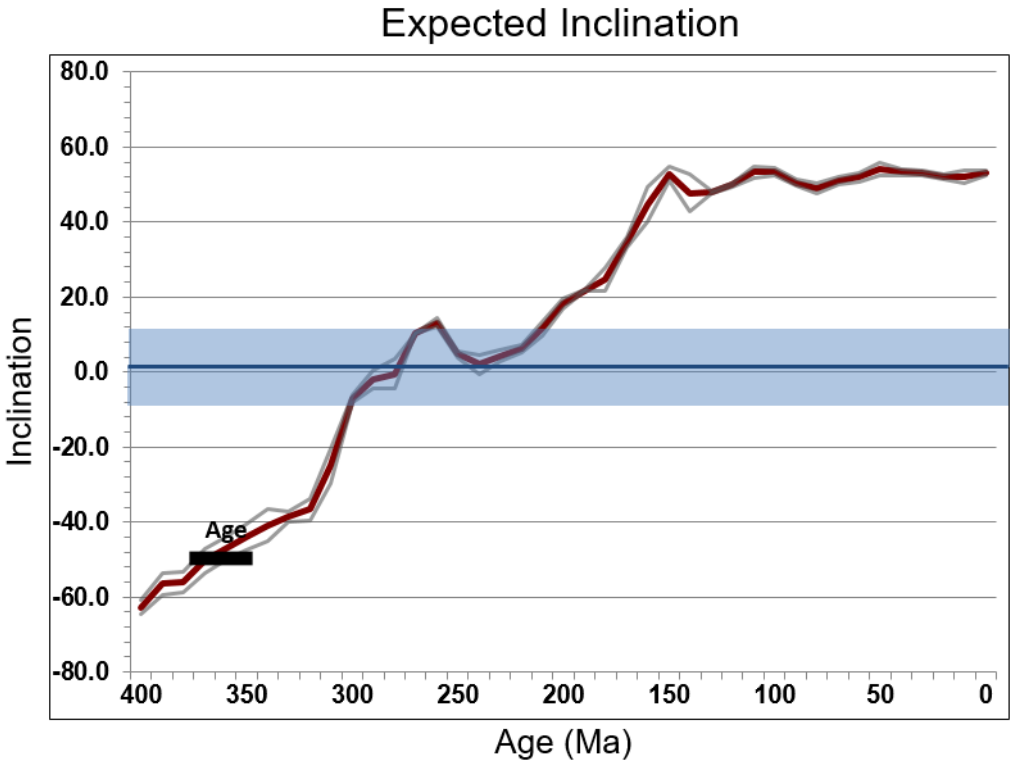

Expected inclination for the location of Core B through geologic time. The red line is the expected inclination; the blue line is the inclination of the ChRM in Core B. The grey lines and the blue rectangles represent the possible error in calculation. The age of the Woodford is indicated on the inclination plot. The ChRM inclination intersects the graph from approximately 285 – 245 Ma. This age is consistent with the findings of the apparent polar wander path (APWP) dating method (Ch. 2, Fig. 6), which yields an age of 250 ± 20 Ma for the ChRM.